

Porous Silicon: Morphology and Formation Mechanisms

Gregory X. Zhang

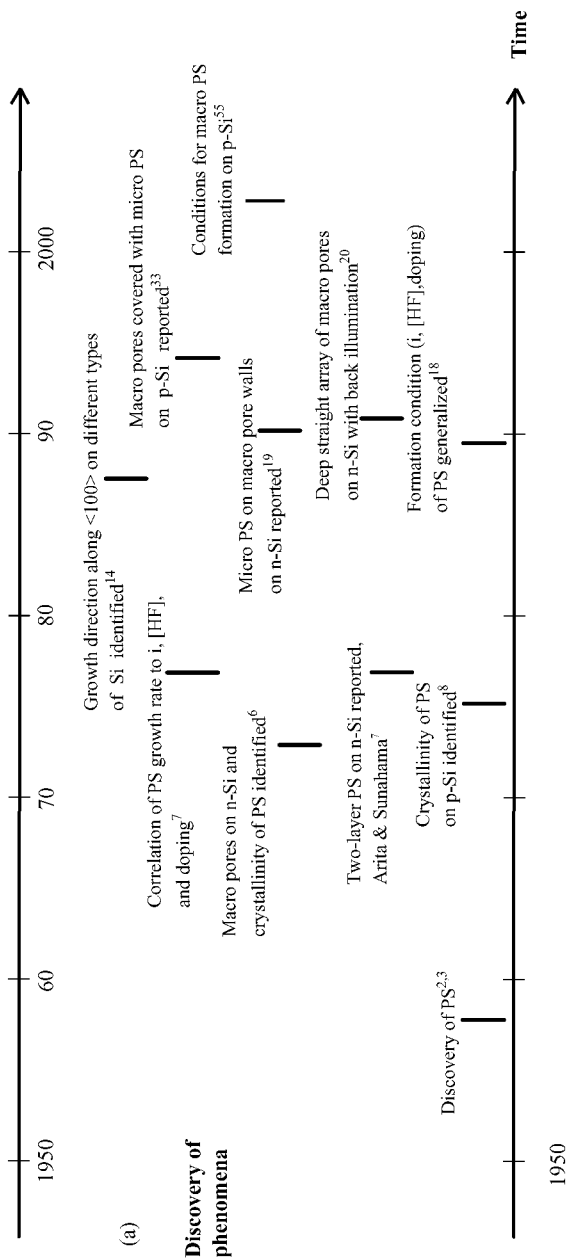
Teck Cominco, Product Technology Centre, Mississauga, Ontario, Canada

I. INTRODUCTION

Porous silicon (PS) is a material formed by anodic dissolution of single crystalline silicon in HF containing solutions. Since its discovery more than four decades ago, a large number of investigations have been undertaken, the results of which revealed that PS has extremely rich morphological features and the formation process of PS is a very complex function of numerous factors.¹ Accordingly, many theories have been proposed on the various mechanistic aspects on formation and morphology of PS. Figure 1 is a summary of the progress of research on PS with respect to the discovery of major PS features and development of theories.

Uhlir and Turner^{2,3} first reported in the late 1950's that silicon surface can be covered with a brown film during anodization in HF solutions and suggested that the film was a subfluoride (SiF_2)_x grown on the surface during the anodic dissolution. Later, Memming and Schwandt proposed that the

Modern Aspects of Electrochemistry, Number 39, edited by C. Vayenas et al., Springer, New York, 2005.



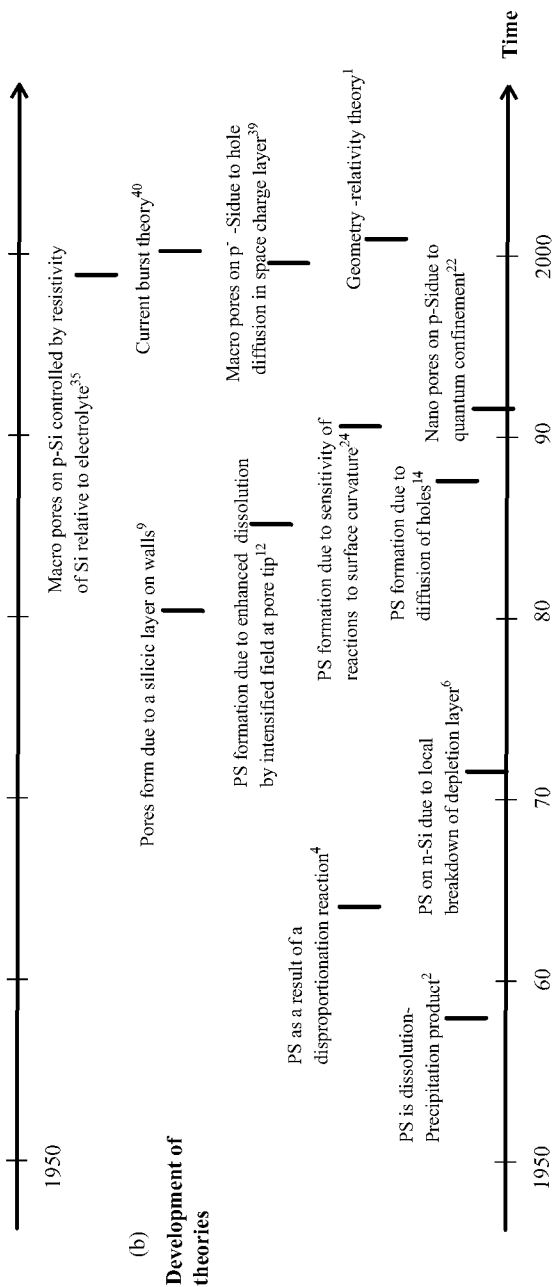


Figure 1. Progress in the discovery of morphological phenomena and in the development of theories on formation mechanisms of porous silicon.

brown film was a dissolution/precipitation product ($\text{Si}^0_{\text{amorphous}}$) resulted from a two-step disproportionation reaction.⁴

The formation of etch pits and tunnels on n-Si during anodization in HF solutions was reported in the early 1970's. It was found that the solid surface layer is the remaining substrate silicon left after anodic dissolution. The large current observed on n-Si at an anodic potential was postulated to be due to barrier breakdown.^{5,6} By early 80's⁷⁻¹¹ it was established that the brown films formed by anodization on silicon substrate of all types are a porous material with the same single crystalline structure as the substrate.

Many theories on the formation mechanisms of PS emerged since then. Beale et al.¹² proposed that the material in the PS is depleted of carriers and the presence of a depletion layer is responsible for current localization at pore tips where the field is intensified. Smith et al.¹³⁻¹⁵ described the morphology of PS based on the hypothesis that the rate of pore growth is limited by diffusion of holes to the growing pore tip. Unagami¹⁶ postulated that the formation of PS is promoted by the deposition of a passive silicic acid on the pore walls resulting in the preferential dissolution at the pore tips. Alternatively, Parkhutik et al.¹⁷ suggested that a passive film composed of silicon fluoride and silicon oxide is between PS and silicon substrate and that the formation of PS is similar to that of porous alumina.

The conditions for formation of PS on all types of substrates in terms of current density and HF concentrations were established by Zhang et al.¹⁸ by the end of 1980's. Whether formation of PS occurs during anodization was found to be largely independent of the electronic properties of silicon such as doping type and concentration, but depend on the nature of electrochemical reactions.

Lehmann and Foll⁹⁻¹¹ in early 1990's reported the formation of straight, smooth and well spaced macro pore arrays on n-Si using backside illumination and surface patterning. They postulated that for these large straight pores the dissolution rate at pore tips are limited by mass transfer in the electrolyte and that the relative rates of carrier transport in the silicon semiconductor and mass transport in the electrolyte determine PS morphology. For the micro pores formed on p-Si, Lehmann and Gosele²²⁻²³ proposed a quantum confinement model; due to the quantum

confinement the pore walls are depleted of carriers and thus do not dissolve during the anodization. At about the same time, Zhang²⁴ proposed the surface curvature model, which postulated that not only the rate but also the distribution of reactions on a curved pore bottom can be greatly affected by surface curvature.

In the late 1990's, Foll et al.⁴⁰⁻⁴³ proposed the current burst theory. The basic hypothesis is that the electrochemical reactions involved in the dissolution of the silicon surface operate in microscopic units. These reaction units have a temporal and a spatial distribution in number and in the state of activity. The formation of pores is due to the synchronization of these operation units at certain time and geometrical scales.

Two-layer PS with a micro PS on surface of a macro PS formed on n-Si under front illumination had been reported in the late 70's but was little investigated until the 90's.²⁶⁻²⁹ The micro PS may have a fractal-like geometry; the structure can vary in the same layer from amorphous to single crystalline and diameter from a few nm to hundreds of nm. It appeared that while the formation of a macro PS layer under front illumination follows the same mechanism as the macro PS formed in the dark, the formation of micro PS is due to the effect of the photo generated carriers. According to Arita³⁰ the drift current due to the photo carriers generated in the depletion layer is responsible for the amorphous-like PS. Alternatively, Clement et al.³¹ suggested that the micro PS formed under illumination could result from shattering of the macro PS into fine filaments due to residual stress.

Formation of macro PS and two-layer PS on lowly doped p-Si in anhydrous organic HF solutions was first reported by Propst and Kohl^{32,33} in the mid 1990's. It was thought to be related to the chemistry of the organic solvents. Macro pores on lowly doped p-Si were later found to also form in aqueous solutions. Walls of the macro pores are not always covered by a micro PS layer.³⁴⁻³⁶ Wehrspohn et al.^{37,38} suggested that a necessary condition for the formation of macro PS on lowly doped p-Si is a higher resistivity of the substrate than that of electrolyte. This idea was soon invalidated as macro PS was also found to occur in electrolyses that have much higher resistance than the silicon substrate.^{34,39} Alternatively, Lehmann and Ronnebeck³⁹ postulated that the formation of macro PS on lowly doped p-Si is due to the

dominant effect of thermionic emission which is sensitive to barrier height rather than barrier width. More recently, Zhang¹ proposed that the formation of macro PS on lowly doped p-Si is due to the non-linear potential distribution in the highly resistive substrate caused by surface curvature.

Some ideas have been elaborated with extensive mathematical formulation. For example, a theoretical modeling based on charge transfer kinetics for PS morphology was attempted by Jaguiro et al.⁴⁴ Similar mathematical modeling considering the transport phenomena of carriers in the semiconductor, ions in the electrolyte and surface tension was proposed by Valance.⁴⁵ An analytical formulation based principally on thermodynamical arguments was offered by Monica et al.⁴⁶

Most theories have dealt only with certain aspects of the very complex morphology and formation of PS. No single theory is yet close to a globally coherent description of the extremely rich and complex nature of the reactions and the resulting morphological evolution of the silicon electrode surface involved in the formation of PS.¹ Also, these theories on PS did not take into account for the many details of anodic electrochemical reactions and processes of the silicon electrolyte interface, which had been extensively investigated. However, a complete description of the diverse morphological features of porous silicon requires the integration of the all the morphological aspects as well as the fundamental electrochemical reaction processes involved in silicon/electrolyte interface. Any theory for the mechanisms of porous silicon formation without such a global integration will be limited in the scope of its validity and the power to explain morphological details. In addition, a globally and microscopically accurate model also requires the full characterization of all the morphological features of PS.

A detailed and comprehensive review on all aspects of the fundamental and applied electrochemistry of silicon/electrolyte interface was provided in a recently published book.¹ The objective of this paper is to provide a conceptual analysis of the mechanisms for the morphology and formation of porous silicon using the large body of the information assembled in the book and to provide an integrated view of the formation mechanisms that can be coherent with the various morphological features on the

one hand and with the understanding of the fundamental anodic reaction processes on the other.

II. FORMATION OF POROUS SILICON

1. I-V Curves and Formation Condition

The formation condition for PS can be best characterized by i-V curves. Figure 2 shows a typical i-V curve of silicon in a HF solution.⁵⁶ At small anodic overpotentials the current increases exponentially with electrode potential. As the potential is increased, the current exhibits a peak and then remains at a relatively constant value. At potentials more positive than the current peak the surface is completely covered with an oxide film and the anodic reaction proceeds through the formation and dissolution of oxide, the rate of which depends strongly on HF concentration. Hydrogen evolution simultaneously occurs in the exponential region and its rate decreases with potential and almost ceases above the peak value.

Porous silicon forms in the exponential region but not at potentials higher than that corresponding to the current peak, J_1 . Electrochemical polishing occurs at potentials higher than the peak potential. At the potentials above the exponential region and below the potential of the current peak, PS formation also occurs, but the PS layer does not completely cover the sample surface.¹⁸ The surface coverage of PS decreases as the potential approaches the peak value. The different regions are similar for other fluoride containing solutions of various compositions and pH values.^{4,52,57,58}

The characteristics of the i-V curves are largely identical for all types materials except for non-heavily doped.^{5,18} For non-heavily doped n-Si, it requires a large polarization or illumination to generate anodic reaction as the surface is under a reverse bias as shown in Figure 3.¹⁸ The i-V curves may not show the clearly defined regions as on other types of Si with a positive potential scanning rate. Different regions can be revealed on the curve measured at certain negative scanning rate. Also, the current density on n-Si is very sensitive to surface roughness.^{6,51}

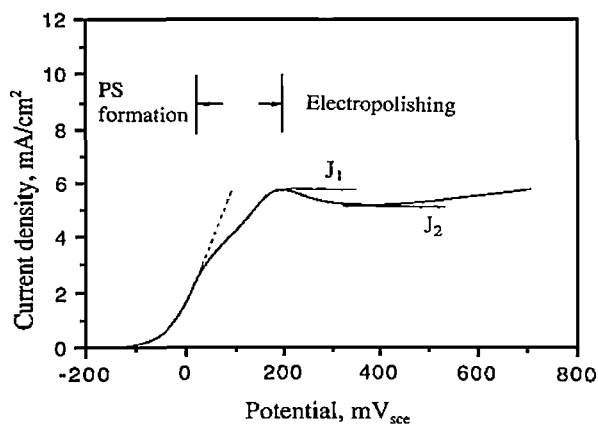


Figure 2. Typical anodic i-V curve measured on a moderately doped p-Si in 1% HF solution.¹⁸

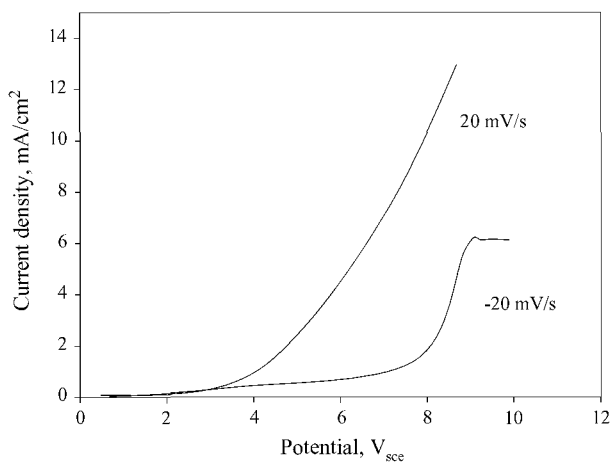


Figure 3. i-V curves of n-Si in 1% HF solution.¹⁸

Mechanical roughening can greatly increase the current density at a given potential. Current can arise on a rough surface at a potential several volts lower than that on a smooth surface.

Anodic dissolution of n-Si can also proceed at a polarization under illumination. The maximum current is limited by illumination intensity when the saturation photo current density is lower than the critical current, J_1 . The characteristics of i-V curves of n-Si under a high illumination intensity, when the reaction is no longer limited by the availability of photo generated carriers, is identical to that for p-Si. Similar also to p-Si, formation of PS on n-Si occurs only below the critical current, J_1 .²⁴

The dependence of i-V characteristics on doping is an indication of the carrier conduction mechanisms that can occur in a silicon substrate. When carrier supply in the silicon substrate is not rate limiting, i-V curves obtained in different HF concentrations are identical in characteristics.⁵⁶ When the supply of carriers in the substrate is rate limiting as determined by the doping and illumination condition, i-V curves display distinct difference between p-Si and n-Si, and for n-Si between illuminated and non-illuminated materials. For non-heavily doped p-Si, the process is by thermal emission of holes while it is by Zener tunnelling for heavily doped materials.^{10,59} For moderately doped n-Si the reaction is limited by the minority holes; significant current occurs when a large amount of holes are generated by illumination or when relatively high anodic potentials are applied to allow interface tunneling to occur.^{11,62}

Examination of the sample surfaces that are anodized at different potentials indicates that the potential corresponding to the maximum slope of the i-V curve is the upper limit for formation of a porous silicon layer that covers uniformly the entire surface. At potentials between the maximum slope and current peak, porous layer may still form but the surface coverage is not uniform. Plotting the current at the maximum slope and the peak current for different types of silicon as a function of HF concentration, the condition for occurrence of PS formation and electropolishing is obtained as shown in Figure 4.¹⁸ This figure also shows that the three regions in relation to current density and HF concentration are essentially independent of the silicon substrate doping type and concentration. This means that the

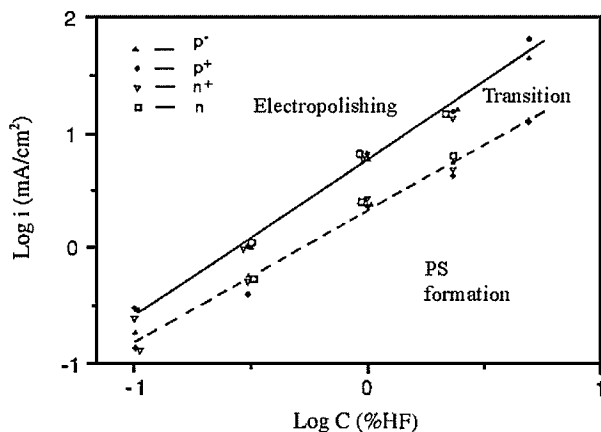


Figure 4. Formation condition for porous silicon; solid line - peak current density, dotted line - current density at the maximum slope (see Figure.2).¹⁸

differences in semiconducting properties of the silicon samples have little effect on the occurrence of these regions. The various parameters involved in PS formation such as potential, doping, and illumination, affect the occurrence of different regions through their relation to the current density. Low current density and high HF concentration favour PS formation while high current and low HF concentration favours polishing.

Electropolishing region does not occur in anhydrous organic solutions due to the lack of water which is required for the formation of oxide film. Figure 5, as an example, shows that in anhydrous HF-MeCN solution the current can increase with potential to a value of about 0.5 A/cm^2 without showing a peak current. The relationship between current and potential is linear due to the rate limiting effect of resistance in solution and silicon substrate.

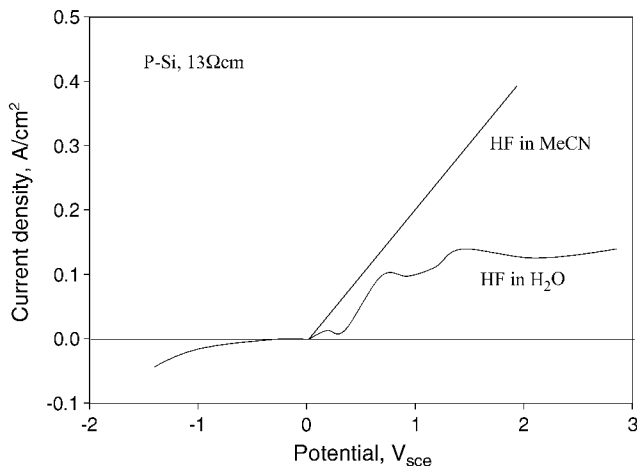


Figure 5. i-V behavior of p-Si in 2M HF + 0.25M TBAP in MeCN and in 2M HF + 1M NH_4F in H_2O , After Propst and Kohl.³³

2. Hydrogen Evolution and Effective Dissolution Valence

Evolution of hydrogen gas occurs during the formation of PS in aqueous solutions. The amount of hydrogen gas is proportional to the time of anodization.⁴ Due to hydrogen evolution, which is a chemical reaction, the effective dissolution valence of silicon, n , can vary between 2 to 4 depending on the relative contribution of this reaction. In general, n increases with increasing anodic current density as the amount of hydrogen evolution reduces; the change is sharpest near the peak current density J_1 . At a given current density, n increases with HF concentration. Also, dissolution valence decreases with increasing PS layer thickness. Dissolution valence as low as 0.5 can be measured for thick PS films formed at low current densities. The low n values are due to chemical dissolution of PS during the time of its growth. The thicker the PS layer the longer the sample is in the electrolyte and the larger the amount of chemical dissolution. This effect is particularly significant for the PS formed on p-Si, which has extremely fine pore structure and thus large surface area.

The formation of hydrogen does not occur in anhydrous organic solvents.^{32,33,63} Due to the lack of hydrogen evolution, dissolution valence is near 4 at all current densities. Addition of water in the organic solvents reduces the dissolution valence.

3. Growth Rate of Porous Silicon

The growth rate of a PS layer can vary over a wide range depending on formation conditions. It can be as low as a few Å/s and as high as 4000 Å/s.^{7,17} For p-Si the growth rate of PS at a given current density appears to increase linearly with respect to HF concentration and current density.^{7,64} For n-Si the growth rate increases also with HF concentration and current density but the relations are not linear (Figure 6).^{7,19,65} Also, for p-Si, it increases linearly with logarithmic dopant concentration but for n-Si the dependence of growth rate on dopant concentration is more complicated. Temperature of HF solutions generally has little

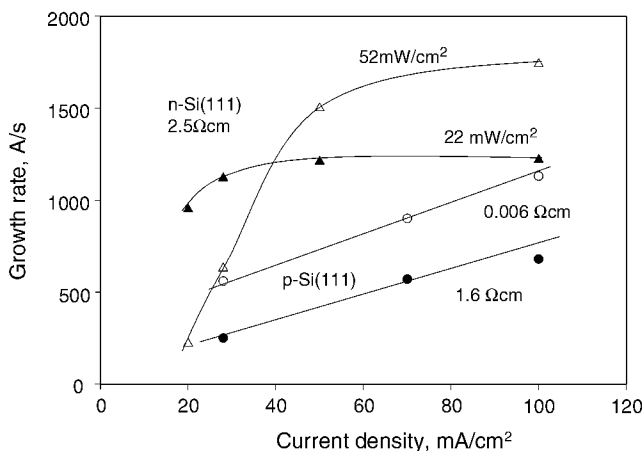


Figure 6. Effect of current density on PS formation rate, after Arita and Sunahama.⁷

influence on growth rate of PS.^{2,66} PS growth rate is generally higher on (100) substrates than on (111) substrates.⁶⁷

Figure 7 shows that PS thickness increases linearly with time up to certain thickness.^{16,17} Such constant growth rate at a constant current density means that the PS formed is uniform in thickness (Effective surface area remains constant assuming reaction kinetics is the same). At a large thickness the growth may deviate from linearity due to the effect of diffusion in the electrolyte within the pores.^{19,25} It has been found that for a very thick PS layer (150 μm) there is about 20% difference in HF concentration between that at the tips of pores and that in the bulk solution.¹⁹

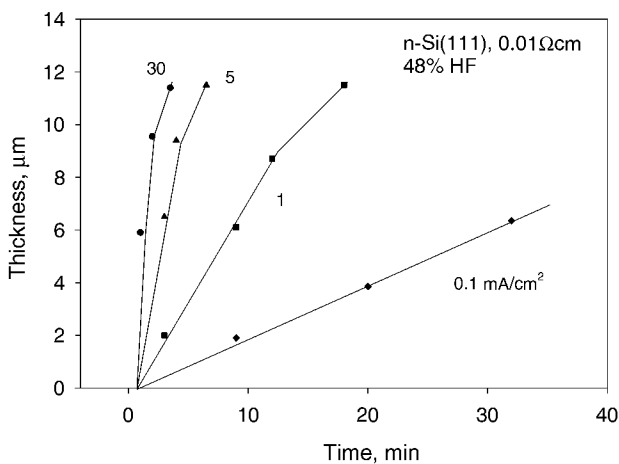


Figure 7. Kinetic dependence of the PS thickness on anodization time, after Parkhutik *et. al.*¹⁷

4. Chemical Dissolution During PS Formation

During PS formation at an anodic potential, the tip of pores dissolves preferentially due to easy excess to holes. The pore wall areas, which are sufficiently distant from the tips, have no holes available, dissolve chemically at a very low rate. The chemical dissolution does not depend on potential but on the time of immersion and the total surface area of the PS. However, although the dissolution rate is very low, a significant amount of material may be removed by the chemical dissolution during the formation period of PS due to the large surface area of PS. Chemical dissolution is responsible for the dissolution valence lower than 2 and the change of PS density with depth. Figure 8, as an example, shows that the amount of chemical dissolution increases with immersion time in the HF solution and with decreasing HF concentration.⁶⁸

The data in Figure 8 can be used to estimate the chemical dissolution rate on the surface of pore walls. For a PS with a density of 50% and an average pore diameter of 3 nm, the chemical dissolution rate is estimated to be about 6×10^{-4} Å/s,

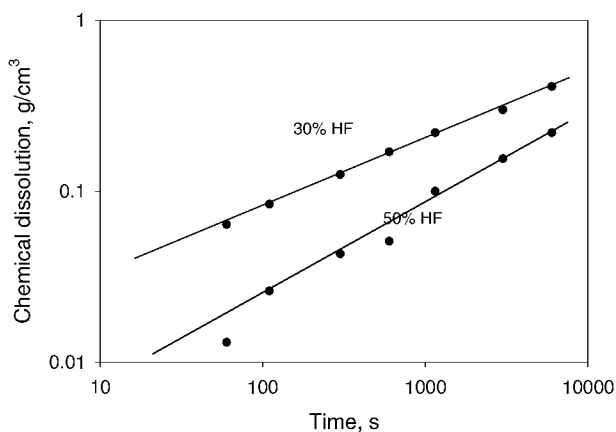


Figure 8 Relationship between amount of dissolved silicon and dipping time in HF solution for the PS formed in 30% and 50% HF, after Unno *et.al.*⁶⁸

assuming the PS consists of straight cylindrical pores of an equal diameter. The order of magnitude is in agreement with the planar etch rate of silicon in concentrated HF solutions.

III. MORPHOLOGY OF PS

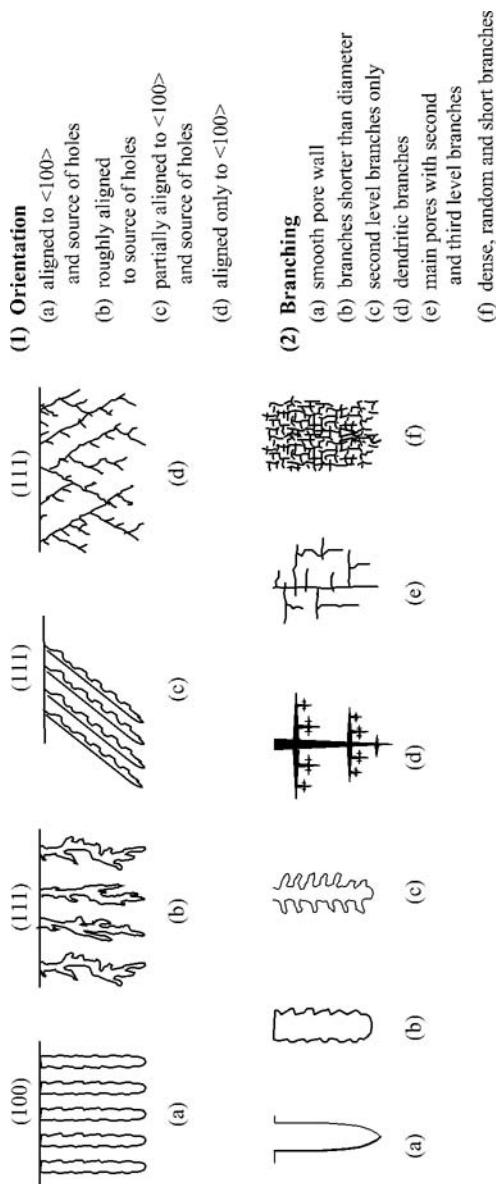
Morphology, which is determined by the distribution of materials in space, is the least quantifiable aspect of a material. It is thus very difficult to characterize morphology of PS, which has extremely rich details with respect to the range of variations in pore size, shape, orientation, branch, interconnection, and distribution. Qualitatively, the diverse morphological features of PS reported in the literature can be summarized by Figure 9 with respect to four major different aspects: pore orientation, fill of macro pores, branching, and depth variation of a PS layer.

1. Pore Diameter

Among the morphological features, the average pore diameter of a PS, as a quantifiable and easily measurable parameter, is most commonly determined. Table 1 shows some examples for pore diameter and interpore spacing reported for the PS formed under various conditions. The pores are categorized in this following text as micro pores (less than 10 nm) and macro pores (larger than 50nm). Pores with size between 10 and 50 nm are grouped into either micro or macro pores depending on the specific situation.

(i) Effect of Doping

The diameter of pores and interpore spacing may vary with doping type and concentration in a wide range, from about 1 nm to about 10 μm , about 4 orders of magnitude.^{14,73,80,81} The PS formed on different substrates can be roughly grouped into four main categories according to doping concentration: 1. moderately doped p-Si (10^{15} - 10^{18}); 2. heavily doped materials, p^+ -Si and n^+ -Si ($> 10^{19}$); 3. non- heavily doped n-Si ($< 10^{18}$); and 4. lowly doped p-Si ($< 10^{15}$). The PS formed on moderately doped p-Si has extremely small pores ranging typically from 1 to 10 nm. For heavily doped p and n types, the pores have diameters



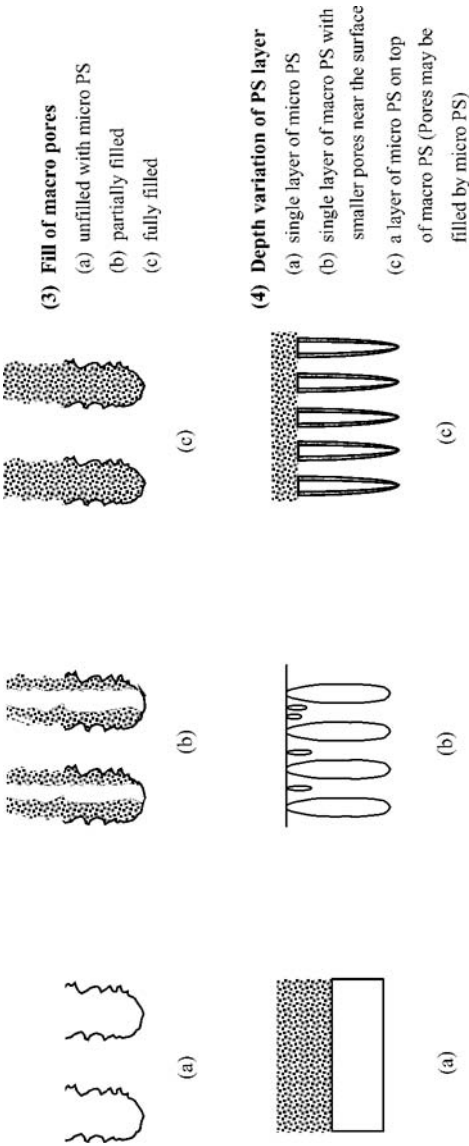


Figure 9. Morphological characteristics of porous silicon.

Table 1
Examples of Pore Diameter, Interpore Spacing and Pore
Density of the PS Formed under Different Conditions (a More
Extensive List is Given in Ref.¹)

Material Ω .cm	Solution % HF	Current mA/cm ²	Diameter μ m	Spacing μ m	Ref.
p (100)					
0.001	20	100	0.05	0.01	59
0.006	33	50	0.005		69
0.006	24 + 47% eth	200	0.002	0.0015	70
0.01	10	10	0.0052		60
0.01	69	30	0.006	0.015	71
0.02	25 + 50% eth	30	0.05	0.02	72
1	49	30	0.003		71
13	2 M HF + MeCN	7	1-2	2-3	33
20	3	2	1.5-3, MP ^c	1-3	39
25	48	10	0.0025		12
50	10	3	2.4-4, MP	1-2	39
100	25	20	3-6, MP	0.5	73
224	2 M HF + MeCN ^b	7	1-2	0.5-2	32
(111)					
10	50	20	0.004		74
10	50:etha.(1:3)	20	0.004		74
(110)					
0.01	49	2	0.005		14
0.4	24 + 47% eth	50	0.035	0.01	70
n-Si (100)					
0.002	1	4	0.05	0.05	65
0.007	15	65	0.004		60
0.01	5	0.1 V, 15 mA, illu.	1-4	0-4	27
0.03	4	4	0.05	0.3-0.8	75
0.1	49	80	0.06		76
0.1	5	6 V	0.14	0.44	24
0.1	20	50	0.009	0.03	77
0.1	20:60, HF:eth	50 mA	0.08	0.1	59
1	2.5	0.5, 10 V, illu., B	0.6	6.9	20
3	10:35, HF:eth	1.2 V, 5mA illu.	0.33	1-2	78
5	6	3 V, 10 mA illu.B ^d	2.5	5	19
10	20:60, HF:eth	50 mA	0.8	> 0.5	59
20	2.5	1.5, 10 V, illu., B	2	5.5	20

Table 1
Continuation

Material $\Omega\text{.cm}$	Solution % HF	Current mA/cm^2 (111)	Diameter μm	Spacing μm	Ref.
0.01	12–48	20	0.01		79
0.008	25:50, HF:eth	50	0.01	0.03	80
2.5	50	30, 7 mW	1.5		7
2.5	50	90, 54 mW	1.7		30
(110)					
0.82	49	80	0.01	0.1	13
3	4	4, 1.5 V	2–4	1–2	39

^a B: backside illumination

^b MeCN: acetonitrile

^c MP: macropores of two-layer PS

^d eth: ethanol,

typically ranging from 10 to 100 nm. For non-heavily doped n-Si, the pores have a wide range of possible diameters from 10 nm to 10 μm . For lowly doped p-Si, the PS can have two distinct distributions of pore diameters: large pores with a distribution of diameters in the order of μm and small pores on the order of nm. The effect of doping on pore diameter strongly depends on solution composition, potential and illumination conditions.

Figure 10 shows that for n-Si the diameter of the pores decreases with doping concentration at different current densities.⁸⁰ In contrast, the pore diameter of p-Si of moderate or high doping concentrations decreases with increasing doping concentration. In the transition region (Figure 4), macro pores can form on all types of substrates, in which the silicon surface is partially covered with an oxide film, and the morphology of PS type strongly depends on solution composition.^{18,27,73,75,82,83} The macro pores formed on p-Si in the transition region have been investigated in a recent study in various solutions.⁵⁵

(ii) Effect of Potential, Current and HF Concentration

Pore diameter generally increases with increasing potential and current density.^{9,24,60,80} Figure 10 shows that the diameter of pores formed on both p-Si and n-Si increases with current

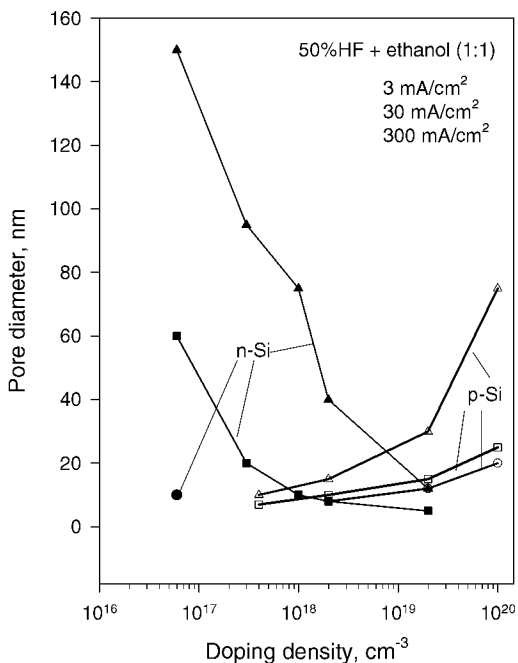


Figure 10. Pore diameter of the PS formed in 5% HF + ethanol (1:1) as a function of doping concentration and current density. After Lehmann, *et.al.*⁸⁰

density over a wide range of doping concentrations.^{60,80} Pore diameter increases, in general, with increasing potential and with decreasing HF concentration.²⁴ The sensitivity of pore diameter to HF concentration strongly depends on solvent.^{8,27,37,39,43} A wider range of pore diameters can be obtained in organic solvents than in aqueous solutions.

(iii) Primary and Branched Pores

As illustrated in Figure 9(2), pores can be straight with smooth walls or can be branched. The branched pores can have

third level or further levels of branches. Branched and hierarchical pore structure has been found to form on all types of substrates. Branched pores are generally smaller than the primary pores.^{12,14,76,84}

(iv) Surface-Patterned Pore Arrays

Straight large pores with smooth walls can be formed by backside illumination of n-Si of (100) orientation.^{19,20,85} Using micro patterning for pore initiation sites on the surface regularly spaced pore arrays can be produced. Production of pore arrays of 2 μm in diameter up to 400 μm deep on 6 in wafer have been reported.⁸⁶ Well aligned pore arrays have not been obtained on (111) and (110) wafers due to the misalignment between the direction of pore growth and that of the hole source.⁸⁷

Under a given formation condition, the pores beyond the surface region have certain size determined by the formation conditions (i.e., HF concentration, current density, potential and doping concentration). According to Lehmann et al.,⁸⁷ the smallest possible pore diameter for a regular pore array formed with surface patterning and backside illumination is about 0.3 μm below which branching at pore bottom occurs; the largest pores are found to be about 20 μm , above which formation of straight and smooth pores becomes a problem due to hydrogen bubble formation.

(v) Variation From Surface To Bulk

The pores at the surface are smaller than those in the bulk of PS as, for example, shown in Figure 11.^{8,16,24} Such an increase in pore diameter from the surface to bulk is due to the transition from pore initiation to steady growth. Also, two-layer PS, a micro PS layer on top of a macro PS can form for on illuminated n-Si or on lowly doped p-Si.^{19,26,78} For the micro PS layer formed on front illuminated n-Si, pore diameter is less than 2 nm and thickness of PS changes with illumination intensity and the amount of charge passed. Also, the diameter of macro pores on front illuminated n-Si changes with the amount of charge Passed.²⁰ Pore size and depth variation of PS on n-Si are very different for front and back illuminated n-Si samples.

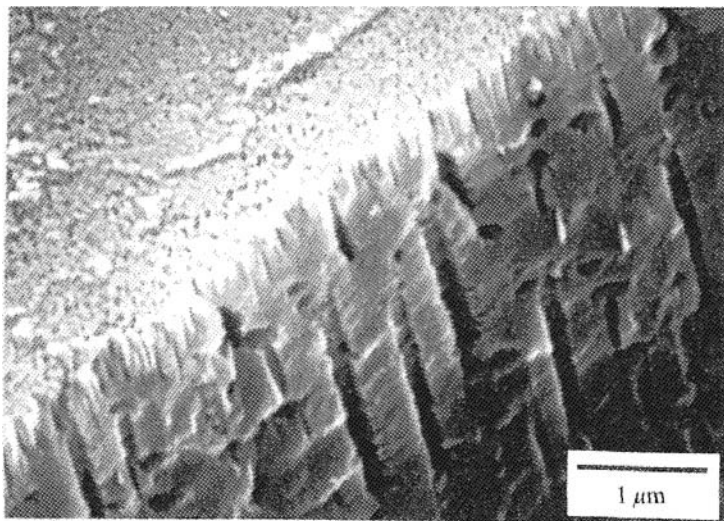


Figure 11. SEM photograph showing smaller pore diameter and larger pore density near the surface than in the bulk in 5% HF at 6 V.²⁴

For very deep pores the diameter may increase with a decreased growth rate due to the effect of diffusion process inside pores. The depth at which this occurs depends on current density and HF concentration.⁸⁷ Low HF concentration, low temperature and low growth rate favour formation of deep uniform pores.

(vi) Interpore Spacing

The variation of interpore spacing or wall thickness is more complex than pore diameter. There is not much information on the relationship between wall thickness and formation conditions. In general, the walls are on the same order as or smaller than pore diameter.²⁴ In particular, interpore spacing depends on potential; it increases with potential at small currents but at certain current it starts to decrease with increasing potential. When interpore spacing is reduced to zero, which occurs in the transition region, pores no longer form, and instead, shallow pits form.

(vii) Distribution of Pore Diameter

Pore diameters of the PS layer formed under a given set of conditions have a distinct distribution. Normal, log-normal, bimodal, fractal, and non-uniform distributions have been found for PS formed under different conditions.^{26,29,60,88,89,90,91}

For the PS formed on heavily doped silicon, pore diameter has a narrower distribution at a lower current at a given HF concentration and the distribution is narrower at a lower HF concentration at a given current density. Bimodal distribution of pore diameter are generally associated with two layer PS on lowly doped p-Si and illuminated n-Si. Pores with multiple distributions have been observed for the PS that has a surface micro pore layer and smaller branched pores in addition to the main pores.^{88,90} Distribution of pore diameters for highly branched PS has been found to be fractal-like.^{14,76} Illumination during formation of PS on p-Si can also affect the distribution of pore diameter; it increases the amount of the smaller nanocrystals, while reduces the amount of larger crystals.⁹² For the PS formed under an illuminated substrate, the relative amount of small crystals tends to increase with reduction of light wavelength.⁹³

2. Pore Orientation and Shape

The growth of individual pores, or the dissolution at pore tips, is anisotropic, depending on the orientation of the substrate and the direction of the carrier source. The relative effect of substrate orientation and direction of the carrier source on the orientation of pores is determined by the specific electrochemical reactions at the pore bottoms.

The orientation of primary pores is in general in the $\langle 100 \rangle$ direction for all the PS formed on all types of (100) substrates.^{7,14,84} For the PS with dendritic structure, as shown in Figure 12, pores propagate along (100) direction even on the (110) and (111) substrates.^{20,84,94} The branched pores of non-dendritic types formed on (100) substrate may not be strictly perpendicular to the primary pores but deviate to various extents from the $\langle 100 \rangle$ direction toward to the source of holes.^{12,14,95} Ronnebeck et al.⁹⁵ found that the macro pores formed on

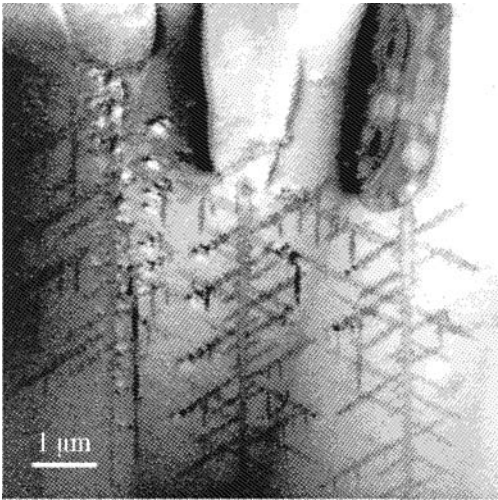


Figure 12. Dendritic PS morphology formed on n (100), 12 Ω cm in 4% HF at 4 mA/cm². After Jäger, *et. al.*⁸⁴

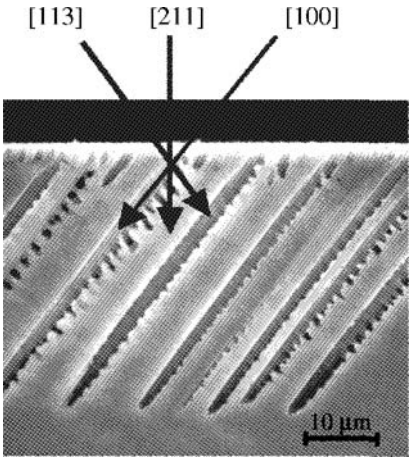


Figure 13. Preferential growth of pore on 35°C from (100) n-Si with back illumination. After Ronnebeck *et. al.*⁹⁵

misoriented $n(100)$ substrates (from 15° to 35°) as well as on $n(111)$ are oriented along $\langle 100 \rangle$ direction when they are formed in the dark at high anodic potentials. However, when the samples are illuminated from the back, the pores formed on the (111) sample and the side pores formed on the 35° misoriented (100) sample are oriented along $\langle 113 \rangle$ as shown in Figure 13.

For pores of extremely small diameters, in the order of a few nm, the direction of individual pores is totally random. On the other hand, large pores tend to have less anisotropic effect and grow more dominantly in the direction of carrier supply, that is, perpendicular to the surface. The macro pores formed on p-Si generally have smooth walls and an orientation toward the source of holes that is perpendicular to the surface, even on (110) and (111) samples.^{34,39}

Depending on substrate orientation and formation condition, individual pores may have different shapes. The shape of the pores formed on (100) substrate is a square bounded by $\{011\}$ planes with corners pointing to the $\langle 100 \rangle$ directions.^{14,77} The shape of individual pores formed on n-Si tends to change from circular to square to star-like and to dendrite-like with increasing potential.²⁰ Low formation voltage tends to favour circular shape while high voltage favours star-like shape. Near perfect square shape of pores can be obtained for the PS formed on n-Si under certain conditions.

The bottom of individual pores is always curved, varying from a shallowly curved semicircle to an elongated conical depending on the formation conditions. As will be discussed later the curvature of pore bottom plays a critical role in the reaction kinetics required for formation of PS and its morphology.

3. Pore Branching

Individual pores, depending on formation conditions, may propagate straight in the preferred direction with very little branching or with formation of numerous side or branched pores. In general, the conditions that favour the formation of small pores also favours branching.

The degree of branching and interpore connection depends strongly on doping concentration. The most highly connected PS

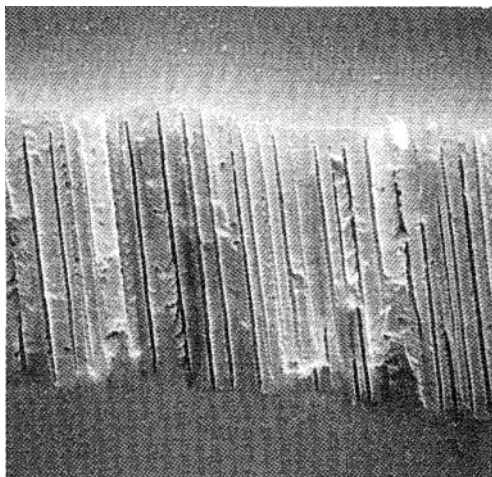


Figure 14. Straight pores with smooth wall formed on n-Si in the dark.¹

is found in the PS of lowly doped p-Si and the micro PS on illuminated n-Si.¹⁴ On the other hand, well separated and straight pores are generally found on moderately or lowly doped n-Si. Perfectly straight pores with smooth walls can be formed on n-Si in the dark, as for example, shown in Figure 14.⁶⁵ Also, on n-Si smooth and straight pores without branching can be obtained under back illumination using surface patterned substrate. For heavily doped materials, pores are generally branched.^{12,71} For non-heavily doped p-Si, pores are highly branched resulting in a random network of pores. The macro pores formed on lowly doped p-Si generally have no side pores longer than the pore diameter.^{32,34,39}

Like main pores, branched pores are highly directional, propagating preferentially in the $\{100\}$ planes and the long $\langle 100 \rangle$ directions.^{14,20,77} Such directional branching can produce regularly spaced three dimensional structures as shown in Figure 15.^{14,65} The tendency to branch is stronger on (110) and (111) substrates than on (100) because for substrates of non-(100) orientations, $\langle 100 \rangle$ direction does not coincide with the direction of the hole source. Due to the large tendency to branch, it is difficult to

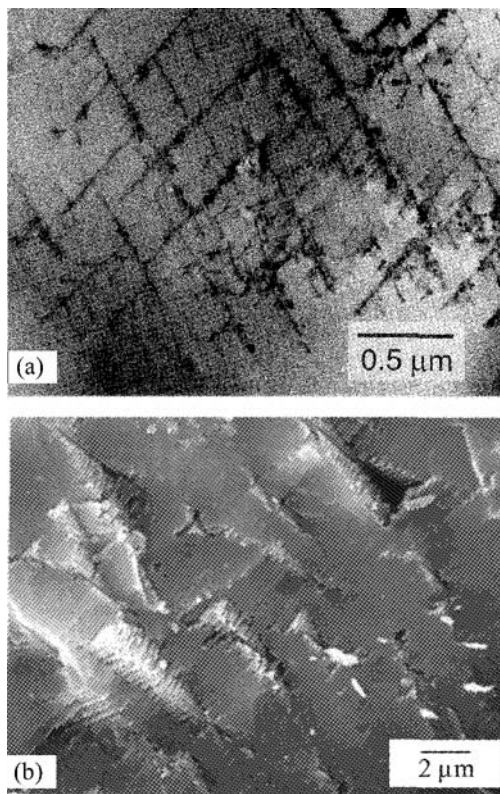


Figure 15. Three dimensional structures generated by the formation of dendritic pores on an n(110) substrate.^{1,14}

produce straight perpendicular pores with smooth walls on (110) and (111) samples, even on surface patterned samples.⁸⁷

4. Interface Between PS and Silicon

The growth of a PS layer (not individual pores) is always perpendicular to the surface of the substrate with back electrical contact. The growth front is planar, independent of the orientation of the silicon samples. The interface between PS layer and silicon

substrate is essentially flat with high and low points deferring within a few microns.

5. Depth Variation

The morphology of PS generally varies in the depth direction from the surface to the bulk. There are two types of depth variations: 1) the change of pore diameter is gradual from the surface to the bulk where pore diameter is constant; and 2) the change of pore diameter is abrupt from a surface layer to the bulk layer with a difference in diameter as large as three orders of magnitude. The surface layer for the first type is a transition layer formed due to the transition from initiation of pores to the steady state growth. The second type is two-layer PS with a micro PS on top of a macro PS. While two-layer PS forms only under certain conditions, the transition PS layer of varying thickness exists on the surface of all PS layers.

(i) *Transition Layer*

Transition layer is found to exist for all types of silicon.^{7,16,20,24,25,80} The pores in the transition layer are generally much smaller than those in the bulk. There is not a clearly definable boundary that separates the surface layer and the bulk. The thickness of the transition layer is related to the size of pores; the smaller the pores the thinner the surface transition layer. For n-Si, the transition layer can be clearly seen as for example shown in Figures 11 and 16.²⁴ On the other hand, for p-Si this surface layer is very thin (near zero) for some PS with extremely small pores. Such thin layer may not be observed because it may be removed due to chemical dissolution during its exposure in solution.

The morphology of the transition layer, unlike the bulk morphology, depends sensitively on surface conditions, particularly surface roughness such as scratches.^{14,94} For n-Si, which usually requires a large potential to generate current in the dark, formation of PS can occur at much lower potentials if the surface is roughened mechanically.

A certain amount of uniform dissolution may occur prior to and during the initiation of pores. Such an etched layer prior to the

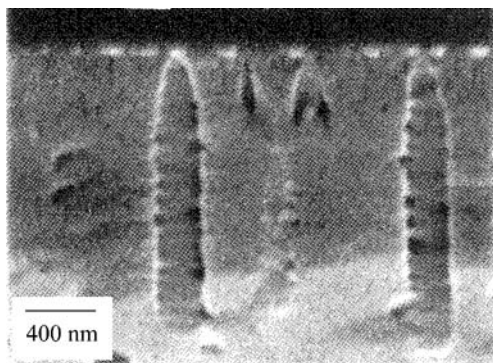


Figure 16. Variation of diameter of pores from the surface to the bulk. After Zhang.²⁴

initiation of pores is involved in all types of PS since the etching, which causes roughening of the surface, is required for pore initiation.^{84,95} The thickness of etched layer is generally in the order of pore diameter.

(ii) Two-Layer PS

Two-layer PS, with a micro PS layer on top of a macro PS layer, forms only under certain conditions. For n-Si, formation of two-layer PS is associated with front illumination, although it can also be formed with back illumination.^{19,27,34,37} For p-Si, two-layer PS are found to form on lowly doped substrates. For moderately or highly doped p-Si or for n-Si in the dark, formation of two-layer PS has not been observed.

Formation of two-layer PS on front illuminated n-Si depends on the wavelength of light; formation of large and deep pores does not occur with a white light at wavelength < 800 nm, but occurs at wavelength > 867 nm.²⁰ This phenomenon is due to the wavelength dependent absorption depth; carriers which are generated deep in the bulk promote pore growth at the tips of macro pores whereas those generated near surface result in the formation and dissolution of micro PS and lateral growth of the macro pores.

There is a correlation between the occurrence of two-layer PS and the saturation photo current value.⁷⁸ Only a single micro PS layer forms at a photo current density below the photo saturation value while two-layer PS forms at current densities above the saturation current as shown in Figure 17. Also, macro PS layer forms only after a certain amount of charge determined by the amount of etch required for the initiation of macro pores.⁷⁷

There is also an etched layer of Si on the surface under illumination as illustrated in Figure 18. This etched layer is mainly due to photo-induced corrosion. As a result of the photo induced dissolution the top surface of PS layer recedes with time. The rate of dissolution depends on doping, HF concentration, current density and illumination intensity.

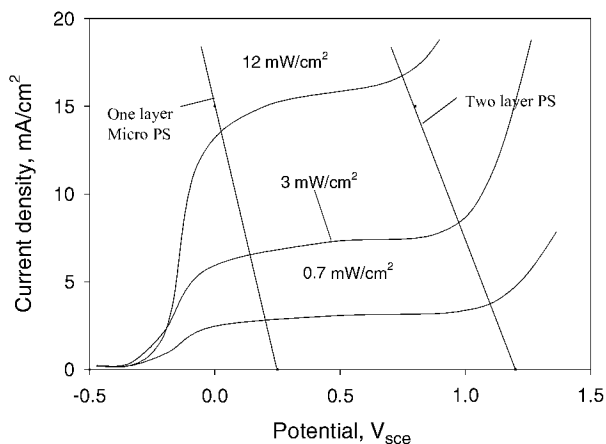


Figure 17. Voltammograms of n-Si electrodes in aqueous solution containing 10 wt.% HF and 35 wt.% C₂H₅OH at 5 mV s⁻¹ under different light intensities. The illumination intensity was adjusted by changing the distance between the light source and the n-Si electrode. After Osaka *et.al.*⁷⁸

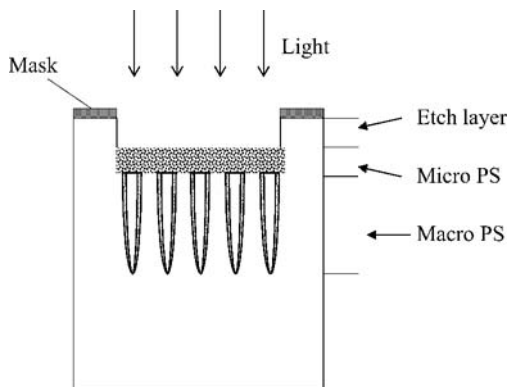


Figure 18. Three layers are resulted after formation of PS on illuminated n-Si sample: an etch layer, a micro PS layer and a macro PS layer. The walls of the macro pores may also be fully or partially covered with micro PS.

The micro PS on top of the macro PS formed on n-Si under illumination can have a very complex structure. It has been reported that the PS formed on n-Si has an irregular and square-shaped framework of pores with interconnected columns of 100-200 nm for lowly doped materials and 100-400 nm for highly doped materials.²⁹ Bounded to this rigid square-shaped framework and contained within is a finer structure with wire-like structures of sizes varying from 3 to 12 nm. Fractal morphology has been suggested to associated with this type of micro PS. The macro pores formed on front illuminated n-Si, once initiated, can increase in diameter with time without reaching a constant value.^{20,27} The diameter of macro pores also increases with increasing HF concentration.

The PS formed on p-Si generally consists of micro pores, but when the resistivity is above a certain value macro pores can form underneath a layer of micro pores.^{34,39,73} The resistivity, at which this occurs, depends on type of solvent, HF concentration and

current density. In aqueous HF solutions macro pores are found to form on substrates of resistivity higher than $5 \Omega\text{cm}$.³⁹ On the other hand, macro pores has been found to form on substrate with a resistivity of $1 \Omega\text{cm}$ in 2M HF + dimethylformamide electrolyte.³⁴ Presence of water in organic solvents tends to reduce the thickness of the micro PS layer.

(iii) Fill of Pores

The macro pores of two-layer PS may be completely filled or only partially filled with micro pores depending on the solution composition.^{39,63} When other conditions are the same, macro pores formed in organic solvents tend to be more filled than those formed in aqueous solutions. Addition of water to organic solutions reduces the extent of filling. Among organic solutions, according to Jager et al.,⁵⁴ the degree of filling of the macro pores formed on p-Si depends on the oxidizing nature of the solutions: macro pores are filled with micro PS in non-oxidizing electrolyte such as acetonitrile (MeCN), while they are not filled for oxidizing electrolytes such as dimethylformamide (DMF).

For the two-layer PS formed on front illuminated n-Si, the degree of filling of the macro pores depends on light intensity, on the amount of charge passed, as well as on the magnitude of the current relative to the saturation photo current.^{26,27,29,78} The thickness of micro PS increases with the amount of charge passed and it decreases with increasing light intensity.²⁷ The macro pores formed on lowly doped n-Si under back illumination can also be filled by micro PS and the degree of filling decreases with increasing potential.¹⁹

6. Summary

The morphology of PS has extremely rich details determined by the numerous factors involved in the anodization. Generally, p-Si and n-Si have distinct differences in the correlation between PS morphology and formation conditions. Among all formation conditions doping concentration appears to show the most clear functional effect on morphology. A summery of morphology features of PS is provided in Table 2.

Table 2
Morphological Characteristics of Porous Silicon^a

Size
<ol style="list-style-type: none"> 1. A PS layer may have one or two distinct distributions of pores with sizes varying from 1 nm–10 μm. Those less than 10 nm are micro pores and those larger than 50 nm are macro pores. In the dark moderately doped p-Si (10^{15}–10^{18}): one distribution, 1–10 nm. heavily doped p-Si and n-Si ($> 10^{19}$): one distribution, 10–100 nm. non-heavily doped n-Si ($< 10^{18}$): one distribution, 10 nm–10 μm. lowly doped p-Si ($< 10^{15}$): one or two distributions, 1–10 nm and $> 1 \mu$m. Illumination Little effect on p-Si. For n-Si, one or two distributions 1–10 nm and 50 nm–10 μm. 2. For p-Si pore diameter increases with doping concentration; for n-Si, it decreases with doping concentration. 3. It increases with potential or current density but decreases with HF concentration. 4. Branched pores are smaller than primary ones. 5. It is constant in the bulk but is smaller near the surface. 6. Inter-pore spacing can be smaller than pore diameter but is not larger than three times the diameter. It varies with the factors similarly as pore diameter.
Orientation
<ol style="list-style-type: none"> 1. Pores grow preferentially along $\langle 100 \rangle$ directions and toward the source of holes. 2. Well aligned macro pores, > 50 nm are perpendicular to the surface for (100) substrate but may have a less than 90° angle to the surface on other substrates. 3. Pores can be fully aligned with $\langle 100 \rangle$ directions or/and with source of holes. Pores with smooth wall tend to be aligned with source of holes, while dendritic pores are aligned with $\langle 100 \rangle$ directions. 4. Very small pores, < 10 nm, do not show clear orientations.
Branching
<ol style="list-style-type: none"> 1. PS has discrete pores with no branches, with short branches, or with dendritic branches, or have no primary but densely and randomly branched pores. 2. Tendency to branch increases with decreasing pore diameter. 3. Direction of branching has the same tendencies as pore orientation.
Fill of pores
<ol style="list-style-type: none"> 1. In PS of two distributions, macro pores may be partially or fully filled by micro pores. 2. It tends to occur in organic solvents; addition of water reduces the extent of filling. 3. Extent of filling decreases with increasing light intensity or increasing potential.

Table 2. Continuation

Depth variation	
1.	Two types: transitional layer, which has no clear boundary with bulk and two layer type with clear boundary between micro and macro PS layers.
2.	Transitional layer is associated with the initiation of pores with smaller pores at the surface.
3.	Two layered PS occurs only on illuminated n-Si and lowly doped p-Si.
4.	Pore diameter and distribution is uniform in the bulk of PS.
Others	
1.	The bottom of pores is curved with the smallest curvature at the tips.
2.	The shape of pores can be square, dendritic, circular, and star-like.
3.	Interface of PS/Si is flat and is perpendicular to the source of holes.
4.	PS with macro pores has the same composition and crystalline structure as the substrate; PS with micro pores can be amorphous and highly hydrogenated and/or oxidized.
5.	Pore wall is rough at atomic scale for all pores.

^a Based on information summarized in Ref. ¹.

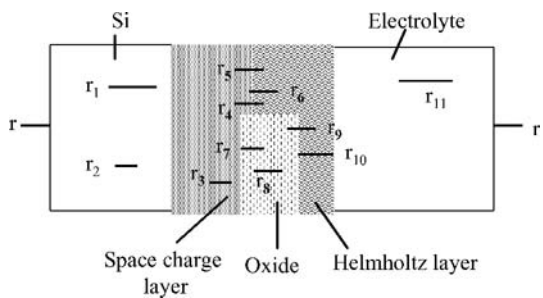
IV. ANODIC REACTION KINETICS

1. Potential Distribution and Rate Limiting Process

There are five possible physical phases in the current path in which the current conduction mechanisms are different as illustrated in Figure 19. They are substrate, space charge layer, Helmholtz layer, surface oxide film, and electrolyte. The overall change in the applied potential due to a change of current density in the current path is the sum of the potential drops in these phases:

$$\Delta V_{\text{app}} = \Delta V_{\text{Si}} + \Delta V_{\text{s}} + \Delta V_{\text{H}} + \Delta V_{\text{ox}} + \Delta V_{\text{el}} \quad (1)$$

The distribution of the applied potential in these different phases depends on silicon material as well as potential range. Table 3 is a summary for the potential distribution of different materials in the three potential regions (Figure 2). While the distribution of the potential below the passivation potential V_{p} (potential at current peak J_1 in Figure 2) depends on doping type and concentration,



- r_1 & r_2 - majority & minority carrier transport,
- r_3 - transport of holes to the surface
- r_4 - charge transfer across the Helmholtz layer,
- r_5 - electron injection
- r_6 - chemical dissolution,
- r_7 - oxide formation,
- r_8 - ionic transport in oxide,
- r_9 - injection of oxidants,
- r_{10} - dissolution of oxide,
- r_{11} - mass transport in electrolyte

Figure 19. Schematic illustration of the processes involving the transport of charge and species in the different phases in the interface region.

Table 3
Distribution of the Applied Potential in the Electric Layers at the Silicon/Electrolyte Interface in HF Solutions

Material	OCP to V ($i \sim 0$) ^a	Exponential region	V > V _p
Heavily doped p, n-Si	Helmholtz layer	Helmholtz layer	Oxide film
Non-heavily doped n-Si	Space charge layer	Space charge layer	Oxide film
Non-heavily doped p-Si	Space charge layer	Helmholtz layer & space charge layer	Oxide film

^aOCP, V ($i \sim 0$), V_p: defined in Figure 2.

the applied potential is principally dropped in the oxide film at a potential higher than V_p for all materials.

For n-Si the applied potential is predominantly dropped across the space charge layer in the semiconductor. For p-Si and heavily doped n-Si, distribution of potential is partitioned between the Helmholtz layer and/or the space charge layer.^{18,48-51} For heavily doped materials the surface is degenerated and the material behaves like a metal electrode, meaning that the charge transfer reaction in the Helmholtz double layer is the rate determining step and potential drops mostly in the Helmholtz layer. For non-heavily doped p-Si, the potential is mostly dropped within the space charge layer before the onset of current. At potentials higher than that at which current becomes measurable, the change in potential may be dropped also in the Helmholtz layer in addition to the space charge layer. Also, for very lightly doped material, potential drop in the substrate can also be significant.⁵²

Because of the different potential distributions for different sets of conditions the apparent value of Tafel slope, about 60 mV, may have contributions from the various processes. The exact value may vary due to several factors which have different effects on the current-potential relationship: 1) relative potential drops in the space charge layer and the Helmholtz layer; 2) increase in surface area during the course of anodization due to formation of PS; 3) change of the dissolution valence with potential; 4) electron injection into the conduction band; and 5) potential drops in the bulk semiconductor and electrolyte.

Each of the possible processes in anodic dissolution of Si, as illustrated in Figure 19, can be the rate limiting process under certain conditions. For example, the anodic reaction processes on n-Si in the dark is limited by the minority hole transport in the bulk of silicon, that is r_2 . For p-Si and illuminated n-Si in fluoride solutions at potentials negative of the first current peak, J_1 , the reaction rate is determined by the charge transfer process across the electrode/electrolyte interface, that is, r_4 and r_5 . At potentials positive of J_1 , i.e., the electropolishing region, the rate determining step is the dissolution of the anodic oxide film, that is r_{10} . The dissolution of the oxide film formed at low fluoride concentrations is mainly kinetically controlled, that is r_{10} , while at high fluoride concentrations the process is mainly diffusion

Table 4
Rate Limiting Steps Involved in the Anodic
Reactions^d

	r^d	p	n	p^+, n^+
Dark				
OCP	~ 0	r_3	r_3	r_3
OCP < $V < V_p$	large	r_4	r_2 or r_5^b	r_4
$V \geq V_p$	large	r_{10}, r_{11}	r_{10}, r_{11}	r_{10}, r_{11}
Illuminated				
OCP	large	r_4	r_3	r_4
OCP < $V < V_p$	large	r_4	r_3 or r_4	r_4 or r_5^c
$V \geq V_p$	large	r_{10}, r_{11}	r_{10}, r_{11}	r_{10}, r_{11}

^a oxidation rate, qualitative comparison to the dark limiting current density

^b it is r_2 below the breakdown potential but it is r_4 above the breakdown potential;

^c it is r_3 when the current equals the saturation photo current, is r_5 when the current is larger than the saturation photo current and is r_4 when the current is less than the saturation photo current;

^d in aqueous solutions containing no redox couples other than the ones associated with HF and H₂O; presence of redox couples can affect the rate limiting process.

controlled, r_{11} . There is a critical concentration, depending on pH, convection and potential, at which the contributions by kinetic and diffusion processes are equal. Table 4 is a summary for the rate limiting steps under various experimental conditions.

2. Reaction Paths

The surface of silicon in HF solution is terminated by hydrogen with or without active dissolution.^{53,54} Thus, dissolution of a surface silicon atom involves first the replacement of a surface hydrogen atom with F⁻ in HF solutions. As shown in Figure 20, replacement of H by F⁻ requires a hole which results in a neutralized Si-F bonding. The valence state of the adsorbed hydrogen before and after the replacement, being zero, is not changed. On the other hand, hydrogen adsorption onto a silicon atom is a reduction process since the valence of the hydrogen atom is changed from +1 to zero. It occurs when the Si-SiF bond

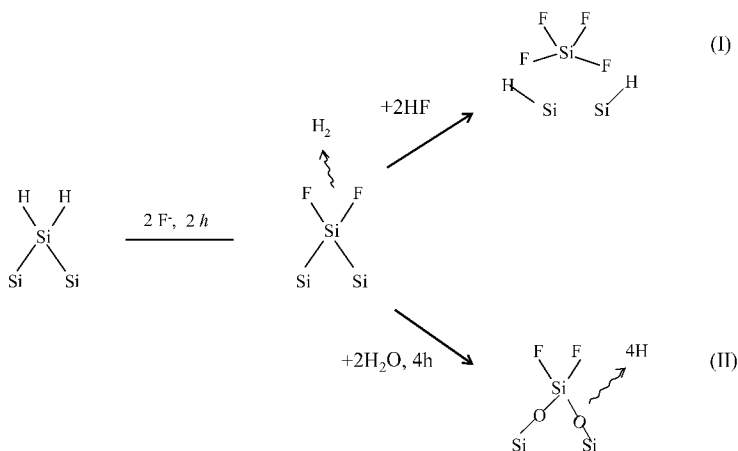


Figure 20. Two different reaction paths for a silicon electrode in HF solution

is broken by reacting with HF (path I). Transfer of one electron from the Si-SiF bond to the hydrogen from a HF occurs to form a Si-H bond.

An important feature of step (2) is that no carriers from the solid are involved although it is an oxidation process for the silicon atom involved (from valence 2 to 4), and it therefore is a chemical reaction in nature. This is the key reaction step responsible for the chemical character of the dissolution process in that in the process of becoming adsorbed a hydrogen ion is reduced by receiving an electron from the Si-SiF bond. Alternatively in the second step, the backbond of Si-SiF can be broken by reacting with H_2O , resulting in Si-O-Si bonds, which are not stable in HF and the dissolution of which results in an indirect dissolution path (path II). Thus, while reaction path (I) results in the direct dissolution of silicon, path (II) results in indirect dissolution. Note also that reaction path (I) results in a dissolution valence of 2 while that of reaction path (II) is 4. As the coverage of the surface by Si-O-Si bonds increases with increasing potential, the surface becomes increasingly less active and becomes passivated when these bonds fully cover the surface

(i.e., formation of a continuous oxide film). Further reaction has to proceed via the breaking of Si-O-Si bonds, the rate of which increases rapidly with increasing HF concentration.

Thus, the occurrence of different regions during anodization of silicon in HF solutions is associated with the two competing reaction paths: direct dissolution of silicon and indirect dissolution through formation and dissolution of silicon oxide. Formation of PS, which is associated with semiconductor property of the surface as will be detailed in a following Section, is only possible when the surface is not fully covered by an oxide film such that direct electrochemical dissolution of silicon is possible. At low potentials, direct dissolution of silicon dominates and PS is readily formed. On the other hand, at potentials higher than the current peak, the entire surface is covered with an oxide film. The dissolution is determined by the properties of the oxide film and no longer by the semiconducting properties of silicon. PS does form under such condition. The formation of an oxide film and its surface coverage determines the occurrence of these three regions shown in Figure 4. (Electropolishing region is absent in anhydrous organic solutions due to the lack of water that is required for the formation of oxide film).

The electrochemical reactions and processes involving the anodic dissolution of silicon in HF solutions have been extensively studied in the past. Table 5 provides a summary for the characteristics of the anodic processes that are relevant to the formation of PS (details are documented in Ref.¹.)

3. Effect of Geometric Elements

The overall formation mechanism of PS must involve the fundamental electrochemical reactions in three essential aspects: 1. nature of reactions, reactants, products, intermediates, number of steps, and their sequences, 2. nature and rate of charge transport in the different phases at silicon/electrolyte interface, 3. spatial and temporal distributions of reactions and the cause of such distributions. The first and second aspects, which governs the properties of a uniform and flat surface and do not involve geometric factors, have been characterized in previous Sections and the major characteristics are summarized in Table 5. This Section deals with the third aspect, that is, spatial and temporal

Table 5
Characteristics of Anodic Processes Relevant to the
Formation of PS

1	In aqueous solutions silicon reacts spontaneously with water to form an oxide film which passivates the surface.
2	Presence of HF results in the dissolution of silicon oxide and activates the surface. Fluoride species such as HF and F ⁻ also react directly with the bare silicon surface.
3	In aqueous HF solution, the dissolution of silicon atoms has two principal competing paths, one via the reaction with HF and the other with H ₂ O.
4	Silicon, having 4 valence electrons, dissolves in multiple steps, each of which may occur at different energy levels and may proceed via the conduction band as well as the valence band depending on the condition of Si/electrolyte interface.
5	The surface of silicon during anodic dissolution is dynamically terminated by hydrogen; the dissolution of silicon atoms proceeds by first forming a Si-H bond.
6	The replacement of the hydrogen by fluoride polarizes and weakens the Si-Si backbond and facilitates the subsequent attack on this bond by HF or H ₂ O.
7	The quantum efficiency of photo electrochemical reactions may vary from 2 to 4; the effective dissolution valence may vary from 2 to 4; and the efficiency of hydrogen evolution may vary from zero to near 1 depending on light intensity and potential.
8	Anodic oxide films formed under different kinetic conditions vary in structure, composition and property (e.g., etch rate) and they change with time during the anodization.
9	The applied anodic potential may mostly or partially drop in the space charge layer or in the Helmholtz layer depending on doping type and concentration as well as on the potential range.
10	The rate of removal of surface silicon atoms by the electrochemical reactions is orientation dependant, lowest on (111) and higher on other orientations.

distributions of reactions in relation to the geometrically dependent elements and events in the system. It is this aspect that determines the specific morphology of PS formed under a given condition. Table 6 is a summary of the effect of geometric factors on the kinetics of spatially distributed reactions responsible for formation of pores and the diverse morphological features of PS.

Table 6
Effect of Geometric Factors on Reaction Kinetics

Geometric factors	Effect on reaction kinetics
Surface curvature	Distribution of carriers and active atoms on surface and thus type and rate of reactions
Surface lattice structure	Density of active surface atoms and reactivity of the surface determined by the crystalline orientation of silicon/electrolyte interface
Pore size	Geometric stability of surface against random perturbations
PS thickness	Mass transport and chemical dissolution of PS
Separation of pores	Distribution of potential in the current paths of neighbouring pores
Location of carrier source	Spatial distribution of carriers at Si/electrolyte interface

(i) Surface Curvature

A particular important property of silicon electrodes (semiconductors in general) is the sensitivity of the rate of electrochemical reactions to the radius of curvature of the surface. Since an electric field is present in the space charge layer near the surface of a semiconductor, the vector of the field varies with the radius of surface curvature. The surface concentration of charge carriers and the rate of carrier supply, which are determined by the field vector, are thus affected by surface curvature. The situation is different on a metal surface. There exists no such a field inside the metal near the surface and all sites on a metal surface, whether it is curved not, is identical in this aspect.

Physically, the sensitivity of reactions to surface curvature can be associated with the space charge layer or the resistance of the substrate. For moderately or highly doped materials, this sensitivity is only associated with the space charge layer because the ohmic potential drop in the semiconductor substrate is very small. However, for lowly doped material a significant amount of potential can drop in the semiconductor to cause the current flow inside semiconductor to be also sensitive to the curvature of the surface.

(ii) Effect of Width of Space Charge Layer

The bottom of all pores is curved, which affects the field at the surface of a semiconductor. For an interface with a spherical shape as illustrated in Figure 21, the field in the semiconductor can be calculated by solving the Poisson's equation.⁸

$$\xi(x+r_0) = \frac{qN_b}{3\epsilon} \left[-(x+r_0) + \frac{(r_0+x_d)^3}{(x+r_0)^2} \right] \quad (2)$$

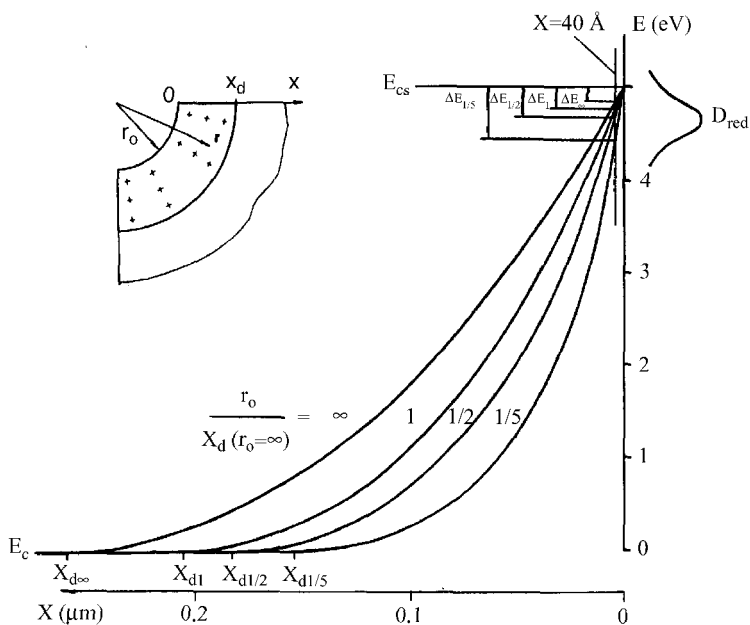


Figure 21. The energy band diagram (only the conduction band is shown) calculated for the silicon/electrolyte interface with a potential drop of 5 V and different radii of curvature. E_c is the conduction band edge in the bulk and E_{cs} is the conduction band edge at the surface. ΔE_4 , ΔE_1 , $\Delta E_{1/2}$, and $\Delta E_{1/5}$ are the possible tunneling energy ranges for different radii of curvature. The distribution of occupied states at the interface, D_{red} , is also schematically indicated. After Zhang.²⁴

strength of a curved surface increases considerably when the radius of curvature is close to or smaller than the width of the space charge layer of a flat surface. Figure 21 shows the effect of in which $r = x + r_0$, N_B is the ionized donor density, q the electronic charge, r_0 the radius of curvature of the interface and x_d the space charge layer width. According to Eq. (2) the field radius of curvature on the energy band diagram with a potential drop of 5 V across the space charge layer of an n-Si under an anodic bias. Clearly the potential drops more sharply for a smaller radius of curvature and the width of space charge layer is considerably reduced. As a result, the field in the space charge layer is greatly increased, for example, the field is about 4 times higher for a curved surface with a radius of curvature of $1/5 x_d (r_0 = 4)$ than that of the flat surface. For n-Si under anodic potentials the current conduction is by electron tunnelling from the surface into the conduction band. Note that the steep band bending due to decreasing radius of curvature increases the number of energy levels for electron tunnelling. In the case shown in Figure 21 the available energy range for tunnelling at a tunnelling distance of 40 Å is about 180 mV for a flat surface while it is about 470 mV for a curved surface with a radius of curvature of $1/5 x_d (r_0 = 4)$.

Similar analysis can be made for other types of materials. Thus, as a generalization, the curvature of a surface causes field intensification, which results in a higher current than that on a flat surface. Although the detailed current flow mechanism can be different for different types of materials under different potentials and illumination conditions, the effect of surface curvature on the field intensification at local areas is the same. The important point is that the order of magnitude for the radius of curvature that can cause a significant effect on field intensification is different for the substrates of different widths of the space charge layer. This is a principle factor that determines the dimensions of the pores.

4. Potential Drop in the Substrate

For a moderately or highly doped material the potential drop due to ohmic resistance in the substrate is very small. For example, for a substrate with a resistivity of $0.1 \Omega\text{cm}$ ($\sim 10^{17}/\text{cm}^3$) the potential drop in the substrate of 0.1 mm thick at a current density of 10

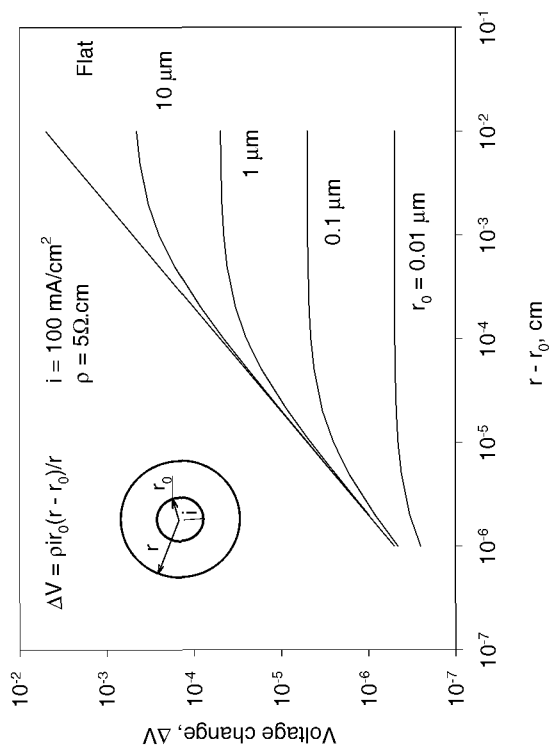


Figure 22. The change of voltage due to resistance of the material in the substrate of a hollow sphere as a function of radius of curvature of the inner sphere.

mA/cm^2 is 0.01 mV, which is insignificant compared to the potential of millivolt range that is required to significantly affect the rate of charge transfer process at the interface. However, when the resistivity is on the order of $10 \Omega\text{cm}$ ($\sim 10^{15}/\text{cm}^3$) or larger the potential drop inside the substrate is in the mV level which starts to affect the distribution of the change of potential in the current path.

For a solid between two spherical surfaces shown in Figure 22, the resistance can be described by

$$R = \rho(r-r_0)/(4\pi r_0 r) \quad (3)$$

where ρ is the resistivity of the material, r_0 is the diameter of the inner sphere and r the outer sphere. The potential drop in the substrate, ΔV_s , for a current $I = i4\pi r_0^2$, where i is the current density on the inner surface, flowing through the solid is then described by

$$\Delta V_s = IR = \rho i r_0 (r-r_0)/r \quad (4)$$

Figure 22 shows that the potential drop in the material with a curved surface increases non-linearly with increasing distance from the inner sphere and most of the potential drop occurs within a distance of a few times the diameter of the inner sphere. Also, for the same thickness of the solid the total potential drop increases with increasing radius of curvature of the inner sphere, reaching the maximum at an infinitely large radius of curvature, that is, a flat surface. The value of the potential drop is in the order of mV for a inner diameter of $10 \mu\text{m}$ under the conditions shown in Figure 22. It will be larger if the current density or the resistivity is higher. Also, the results shown in Figure 22 are for a spherical surface. In the case of curved pore bottoms, which are roughly semi-spherical, the potential drop from individual pore bottom into the solid must be significantly larger than that of an isolated sphere because the current flow from one pore overlaps with those from the neighbouring pores.

The results of the above analysis suggest that the formation of macro PS on lowly doped materials can be associated with a non-linear potential distribution in the solid of a curved surface due to the high resistivity of the solid. The formation of two-layer PS on

p-Si indicates that there are two different physical layers in which the potential-current relations are sensitive to the radius of curvature. The space charge layer of p-Si is thin under an anodic potential and is associated with the formation of the micro PS. The non-linear resistive effect of the substrate is responsible for that of macro PS. Also, to have the same change of potential drop in the substrate, ΔV_s , at a given current density, the radius of curvature must be smaller for a material of larger resistivity according to Eq. (3). This means that the pore diameter decreases with increasing resistivity, which agrees with experimental results.³⁹

As a further deduction, the effect of high substrate resistivity should also occur in the case of lowly doped n-Si. However, the width of the space charge layer in such a substrate under an anodic potential is on the same order of magnitude as the dimension of the resistive layer. Since macro PS forms on n-Si substrate at an anodic potential in the dark, the effect of these two causes on the diameter of the pores formed on n-Si in the dark are not distinguishable under normal conditions. If the conditions can be controlled in such that the pores formed due to the effect of the space charge layer and that due to the effect of the resistive layer have a size difference by at least one order of magnitude it would be possible to obtain the PS with two distinct distributions of pore diameters on high resistivity n-Si. Such a condition might exist at a low potential (small space charge layer thickness) on a back illuminated n-Si substrate. It might even be possible to obtain the PS with three distinct distributions of pore diameters on a front illuminated n-Si sample.

5. Surface Lattice Structure

The surface of a single crystal can have different reactivities depending on the orientation of the surface. For example, the dissolution rate of (100) silicon in alkaline solutions can be many orders of magnitude larger than that of (111) substrate. A major cause of orientation dependent reactivity is the bonding condition of surface atoms. Characteristically, the silicon atoms on (111) surface have three bonds connecting to the substrate lattice while those on (100) surface have only two and are thus have weaker attachment to the surface compared to those on (111) surface.⁹⁹

Also, a real surface has atomic structures associated with roughness and defects and thus the atoms at these lattice structures have different bonding conditions, some are similar to those on a (100) surface in terms of bonding characteristics; some are similar to a (111) surface and others are in between. Thus, a real surface may have varying degrees of reactivity determined by the concentration of the active atoms, which is a function of lattice structure determined by orientation, roughness, and type and density of defects.

The rate of an electrode reaction is a function of three principle types of species: charge carriers on the surface, active surface atoms and reactant species in the solution as illustrated in Figure 23. That is, $r \propto [h] * [Si_{active}] * [A]$. Carrier concentration and reactant concentration do not, in general, depend on surface orientation while active surface atoms may be a function of surface orientation. Anisotropic effect occurs when the rate determining step depends on the active surface atoms that vary with crystal orientation of the surface. On the other hand, reactions are isotropic when the concentration of active surface atoms is not a function of surface orientation or when the rate determining step does not involve active surface atoms.

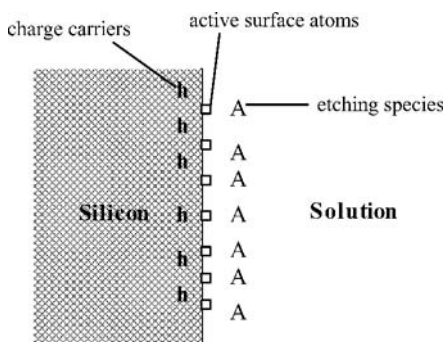


Figure 23. Schematic illustration of the elemental species involved in the dissolution reaction of silicon; h: carries inside the semiconductor, □: active silicon atoms an surface and A: etching species in the solution.

The surface, which is rough at the atomic scale, has no distinct crystallographic character and can be viewed as an amorphous surface as illustrated in Figure 24a. The density of active surface atoms on such surface is similar for different crystal orientations. Thus, when the number of atoms at kink sites, steps and other defects is close to the density of surface atoms, the surface loses its crystallographic nature. For surfaces of such a condition, the difference in reaction kinetics is small for different orientations. On the other hand, when the surface is less rough and has a clear crystallographic character, as shown in Figure 24b, the reaction on the surface is anisotropic when the rate determining step involves the surface atoms. When the surface is covered by an amorphous oxide film, the crystallographic nature of the substrate is masked and the reaction on such a surface is isotropic as shown in Figure 24c. This is the case for electropolishing of silicon electrodes in HF solutions at potentials higher than V_p where the dissolution is through the formation and dissolution of silicon oxide, which is amorphous in structure.

6. Reactions on the Surfaces of Silicon and Silicon Oxide

There are two basic reactions, that is, direct dissolution of silicon via reaction (I) and (II) and indirect dissolution through the formation and dissolution of silicon dioxide via reaction (II). The rates of both reactions increase with potential and proceed simultaneously on the surface of silicon. They compete with each other in rate and coverage of the surface area, and the relative surface coverage of the two reactions depends on the potential. At a low potential the surface coverage of oxide is zero when the rate of reaction (II), which is responsible for the formation of oxide, is low compared to the dissolution rate of the oxide. On the other hand, the coverage is one and the entire surface is covered with an oxide film when the rate of reaction (II) is much higher than the dissolution rate of oxide. Between the two extremes the surface is partially covered with oxide films at local places where the rate of reaction (II) equals the oxide dissolution rate. At low potentials the oxide formation rate is low compared to the dissolution rate and the surface is not covered by an oxide film. Thus, depending on the radius of curvature the bottom of a pore may be covered by an oxide film with varying thickness as shown in Figure 25.

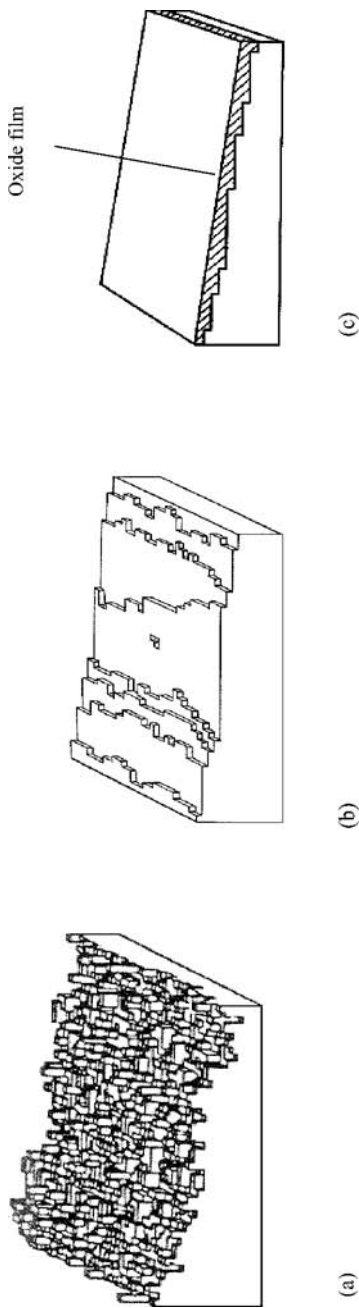


Figure 24. Schematic illustrations of the conditions of surface lattice structure: (a) amorphous-like surface with no identity of orientation, (b) surface with kinks, steps and terraces characteristic of certain crystalline orientation and (c) surface with no identity of the lattice structure of the crystal due to the coverage of an amorphous oxide film.

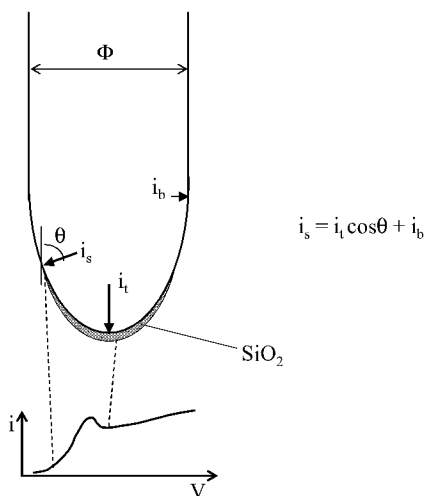


Figure 25. Schematic illustration of current variation and coverage of silicon oxide on the surface of a pore bottom.

Such reactions processes are responsible for the transition from PS formation to electropolishing with increasing potential as typically revealed in an i - V curve.¹⁸ PS formation can occur when the surface is not or only partially covered by oxide. Once the whole surface is covered with an oxide film further reaction can only proceed through the formation of oxide followed by its dissolution. Further increasing the potential will only result in an increase of oxide film thickness. On the other hand, increasing HF concentration will increase the dissolution rate of oxide. The presence of oxide on the silicon surface in the PS formation region and its increase with potential have been experimentally observed.⁹⁸

When the surface is completely covered by an oxide film, dissolution becomes independent of the geometric factors such as surface curvature and orientation, which are responsible for the formation and directional growth of pores. Fundamentally, unlike silicon, which does not have an atomic structure identical in different directions, anodic silicon oxides are amorphous in nature and thus have intrinsically identical structure in all orientations. Also, on the oxide covered surface the rate determining step is no longer electrochemical but the chemical dissolution of the oxide.¹

7. Distribution of Reactions and their Rates on Pore Bottoms

For a stably growing PS the reactions and the rates are different on the pore walls and on the pore bottoms. Furthermore, they are different at different positions of a pore bottom due to the difference in the radius of curvature. The current is the largest at the pore tip because there the radius of curvature is the smallest. It decreases from the pore tip to the pore wall as radius of curvature increases. On the other hand, since the reactions depend on the current density, for a given condition, direct dissolution of silicon dominates at a relatively low current range while oxide formation and dissolution dominate at a higher current range. Thus, oxide formation and dissolution tend to occur at the pore tips at a lower potential than at the side of the pore bottom. There is a distribution of the kind of reactions along the pore bottom.

For a pore to propagate under a steady state the current density on the side of the pore bottom, i_s , and that at the pore tip, i_t , as illustrated in Figure 25 have the relation.

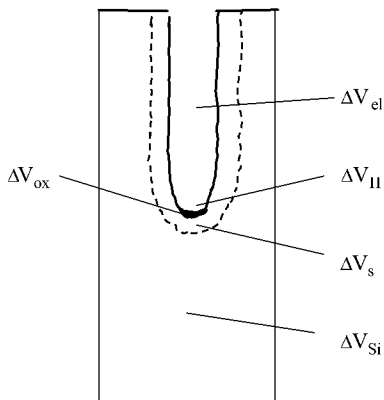
$$i_s = i_t \cos \theta + i_b \quad (5)$$

in which i_b is the extra current mostly due to the anisotropic effect and is responsible for the formation of side pores. The current density at different sites on the bottom depends on θ . It is the largest at the tip where $\theta = 0$, and is the smallest on the boundary of the bottom where $\theta = 90^\circ$. Such a distribution of current density is provided by the distribution of radius of curvature along the pore bottom, which determines the field at the silicon surface and the nature of the reactions. For different HF concentrations and

potentials the current density distribution on the pore bottom is different and so is the shape of the pore bottom. When the pore bottom is curved to such an extent that the current density distribution on the pore bottom for a given HF concentration and a given potential satisfies Eq. (5), pores will propagate stably.

(i) Phases in Current Path

As illustrated in Figure 26, which is a varied presentation for a single pore from the scheme shown in Figure 19, there are five possible phases in the current path in which significant potential drops may occur. The distribution of the applied potential in the different phases of the current path depends on doping type and concentration, HF concentration, current density, potential, illumination intensity and direction. The phases in the current path



$$\Delta V_{app} = \Delta V_{si} + \Delta V_s + \Delta V_{ox} + \Delta V_H + \Delta V_{el}$$

Figure 26. Potential drops along the current path in a pore; ΔV_{si} = potential drop in silicon substrate, ΔV_s = potential drop in the space charge layer ΔV_{ox} = potential drop in oxide ΔV_H = potential drop in the Helmholtz layer, ΔV_{el} = potential drop in electrolyte.

that take large portions of the change in the applied potential, have the consequence of changing current distribution along the pore bottoms, and thus affect the morphology of PS.

The resistance of the electrolyte causes a potential drop that is linearly distributed in the electrolyte inside the pores and thus does not have an effect on the current distribution on the pore bottom. However, the potential drop in the electrolyte has an important effect in maintaining the flat growth front of the PS layer as will be discussed later.

For moderately doped substrates, when the surface is free of oxide the change of potential is mostly dropped in the space charge layer and in the Helmholtz double layer. The reactions are very sensitive to geometric factors. The reaction that is kinetically limited by the processes in the space charge layer is sensitive to radius of curvature, while that limited by the processes in the Helmholtz layer is sensitive to the orientation of the surface. Depending on the relative effect of each layer the curvature effect versus anisotropic effect can vary.

When the pore bottom is covered by an oxide, the change of applied potential occurs almost completely in the oxide due to the very high resistance of the oxide. The rate of reactions is now limited by the chemical dissolution of the oxide on the oxide covered area. When the entire pore bottom is covered with an oxide the rate of reaction is the same on the entire surface of the pore bottom. As a result, the bottom flattens and the condition for PS formation disappears. The change of oxide coverage on the pore bottom can also occur when diffusion of the electrolyte inside deep pores becomes the rate limiting process. Since the current at which formation of an oxide occurs increases with HF concentration, a decreased HF concentration at pore bottom due to the diffusion effect can result in the formation of an oxide on the pore bottom of a deep pore at a condition that does not occur in shallow pores.

When the resistance of the substrate is high and a significant amount of potential is dropped in the substrate, the potential drop may not be uniform along a curved pore bottom due to the non-linear potential distribution on the material surrounding the bottom. Formation of macro PS on lowly doped materials becomes possible under such a condition.

8. Formation Mechanisms of Morphological Features

Formation of PS is due to preferential dissolution of a silicon surface; the rate is larger at some areas of the surface relative to others. Such relative rates with respect to the spatial position of the areas, on which these processes occur, are determined more by the relative nature and less by the absolute nature of the physical and chemical dimensions and events. Specifically, the relative nature of the following aspects is important in determining the morphology of PS:

1. Radius of curvature relative to the thickness of space charge layer
2. Relative depletion of carriers at pore tips to wall region
3. Relative dissolution rate on the (100) surface to that on the (111) surface
4. Density of surface atoms at steps and kinks relative to surface atomic density
5. Relative contribution of the preferential dissolution along direction of carrier source versus that along $\langle 100 \rangle$ direction
6. Relative growth rate of the side pores to that of the main pores
7. Change of profile of pore bottom due to random perturbations relative to pore size
8. Formation rate of oxide film relative to its dissolution rate
9. Rate of direct dissolution of silicon relative to indirect dissolution via oxide formation and dissolution
10. Relative share of potential change among the phases along the current path
11. Potential drop in electrolyte within a pore relative to those within the surrounding pores
12. Distance between surface and source of holes relative to thickness of space charge layer

(i) Pore Diameter and Interpore Spacing

Pore diameter and interpore spacing are determined by two large groups of factors: those that affect carrier density on the surface of a pore bottom and those that affect only the distribution

of the reactions. The first group of factors include doping type and concentration, potential, and illumination direction. The second group of factors include current density, HF concentration, and illumination frequency and intensity.

Except for the macro PS on lowly doped p-Si, both the pore diameter and wall thickness are largely determined by the thickness of the space charge layer. Thus, in general, pore diameter has the same order of magnitude as the thickness of space charge layer. Wall thickness is generally less than twice the space charge layer thickness. Because of the overlapping of the two space charge layers the wall region is depleted of carriers and is thus not conductive. If the wall thickness is larger than twice the space charge layer thickness the walls are not depleted of carriers and dissolution can still occur to form new pores on the walls. Under certain conditions such as backside illumination and surface patterning for n-Si, pore walls can be much thicker than twice the space charge layer thickness because of the favourable position of pore tips for the photo holes generated at the backside.

For a PS formed for controlled space charge layer thickness, the actual wall thickness depends on the relative dissolution rates between the edge of a pore bottom (see Figure 25) and the tip that is between i_b and i_t . If i_b is comparable to i_t , significant dissolution occurs at the edge of the pore bottom before the pore tip propagates far away. This will result in a thin wall or even no wall at all. On the other hand, if i_b is very small compared to i_t , the pore tip will propagate relatively fast so that, before much dissolution occurs on the edge of the pore bottom, the edge has already moved into the wall region where dissolution is virtually stopped due to lack of carriers. This will generate relatively thick walls.

At a given anodic current density, the potential is different for different doping types and concentrations due to different current conducting mechanisms. The combination of doping and potential thus provide a wide range of thickness of space charge layer and thus a wide range of pore diameters. For n-Si the space charge layer and thus the dimension of the pores increases with decreasing doping concentration and with increasing potential. For p-Si, on the other hand, increasing potential reduces the thickness of the space charge layer and results in smaller pores. However, when doping concentration is lower than a certain level,

the effect of substrate resistivity becomes important and formation of macro pores on p-Si can also occur. When this occurs, one obtains a PS with two distributions of pores with a micro PS layer on the surface of macro pores.

It needs to be pointed out that formation of macro pores can also occur on moderately or highly doped p-Si in the transition region (see Figure 4). Formation of macro pores on p-Si in the transition region was first noted on highly doped p-Si in aqueous HF solution¹⁸ and was recently more systematically investigated in various non-aqueous solutions for moderately doped p-Si.⁵⁵ The macro pores formed in the transition region (near the limit of conditions for PS formation) may not be consistent with respect to size and depth from area to area as the coverage of PS may not be uniform on the surface. Also, the pores formed in this region generally have very thin walls relative to the size of pores. The formation of such macro pores can be viewed as a dimensional transition from pores of small radius of curvature in the exponential region to the flat surface that has an infinite radius of curvature. The formation of such large pores is related to the increased coverage of oxide on pore bottoms from the exponential region to electropolishing region. Since formation and dissolution of oxide strongly depend on the amount of water in the electrolyte, the condition for occurrence of the transition region and formation of macro pores on p-Si can greatly vary with type of solution as reported recently.⁵⁵

Under front illumination on n-Si, photo carriers are generated from the surface to the depth of penetration determined by the wavelength of the light. The part of the space charge layer that has a field effect on the photo carriers varies from almost zero to the full thickness of the space charge layer. Correspondingly, the size of pores and wall thickness for the PS formed under illumination may vary from zero (i.e., corrosion of PS) to that comparable to the thickness of the space charge layer, resulting in a fractal-like PS structure.

When the current is larger than certain value, at which oxide starts to form at the tip of pores, increasing current density will increase the coverage of the oxide film on the pore bottom. In such a case the relative change in the current at the pore tip $\Delta i_t/i_t$ with an increase in the current in the pore, Δi , is less than that at the side of the pore bottom, $\Delta i_s/i_s$, that is, $\Delta i_t/i_t < \Delta i_s/i_s$. The

curvature of the pore bottom will increase resulting in larger pores and thinner walls. On the other hand, when the current is relatively small so that the current density at the pore tips is still much less than that required for the formation of oxide, an increase in applied current density will cause a relatively larger increase at the tip than on the side of the pore bottom (The slope of an i - V curve in this current range increases with increasing current density.), that is, $\Delta i_t/i_t > \Delta i_s/i_s$. As a result, the pore bottom becomes sharper with increasing current density. On the other hand, increasing the concentration of HF increases the dissolution rate of oxide, which in turn increases the critical current density at which the surface is covered by oxide. As a result, the pores become smaller and walls become thicker with increasing HF concentration.

(ii) Initiation of Pores

A silicon surface, no matter how well it is prepared, is not perfectly flat at the atomic scale, but has surface defects such as surface vacancies, steps, kinks sites, and dopant atoms. The dissolution of the surface is thus not uniform but modulated at the atomic scale with higher rates at the defects and depressed sites. The micro roughness of the surface will increase with the amount of dissolution due to the sensitivity of the reactions to surface curvature associated with the micro depressed sites. These sites, due to the higher dissolution rates, will evolve into pits and eventually into pores. Depending on the condition, a certain amount of dissolution is required before the initiation of pores on all types of materials.

The pores so initiated are very small in size but large in number due to the nature of surface defects. However, for the bulk PS formed under a steady state at a given anodization condition, the morphology has determined characteristics in terms of pore size, density, branching etc. Thus, the tiny pores initiated on the surface are not stable but tend to grow into the size required for such bulk PS. As the pores propagate into the bulk, some grow gradually in size while some vanish. The thickness of the initiation phase is comparable to the diameter of the pores grown at the steady state. Thus, the initiation layer is very thin for a micro PS and relatively thick for a macro PS.

Although surface defect sites are involved in the initiation of pores they do not determine the density and dimension of the pores in the bulk PS. The bulk morphology of PS is determined by the property of semiconductors and anodization conditions. However, under certain conditions, such as using surface patterning to generate initiation sites, the bulk PS morphology can be controlled to some extent.

(iii) Flatness of the Growth Front of PS

The growth front of a PS layer is generally flat and parallel to the initial surface of the substrate, meaning that the pores, which may have a range of diameters and shapes, propagate at essentially the same rate. This is due to the effect of electrolyte resistance within individual pores. The potential drop in the electrolyte within the pores, ΔV_{el} , plays the critical role of maintaining the same growth rate for different pores. For a pore of length, l , the potential drop in the electrolyte with a resistivity, ρ , inside the pore at a current density i is $\Delta V_{el} = i \cdot \rho \cdot l$. ΔV_{el} is independent of pore diameter and shape but depends on one geometric factor, that is, the length of the pore. Assume one pore is significantly ahead of the surrounding pores, i will increase due to the favourable position of the pore bottom. This will then increase the potential drop inside the pore, ΔV_{el} , which in turn will result in a reduction of the potential available for other phases in the current path. The reduction of the potential in other phases will then reduce the current density and slow down the growth of this particular pore. Thus, due to such a process individual pores can only grow at the same rate and, as a result, the growth front of a PS layer is flat.

(iv) Orientation and Branching of Pores

Orientation, branching and straightness of pores are related to similar factors, namely source of holes and anisotropic effect. Orientation of pores can be explained based on the current difference between (100) and (111) orientations, $\Delta i_{<100>} = i_{<100>} - i_{<111>}$, and the difference between current densities on the pore bottoms of main pores and on side pores, $i_{hole, main}$ and $i_{hole, side}$, as shown in Figure 27. $i_{hole, side}$ is smaller than

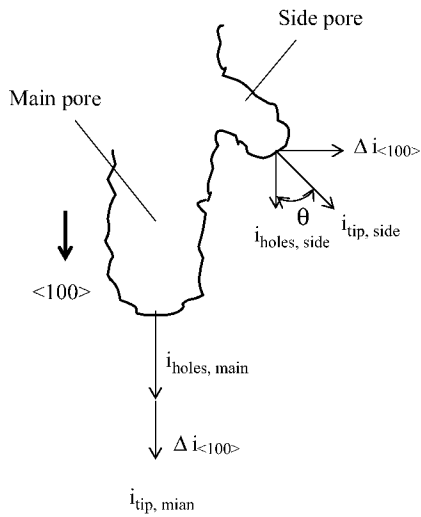


Figure 27. Current components at the tips of main pores and side pores.

$i_{\text{hole, main}}$ due to the unfavourable geometric location. At the tip of main pores, the total current density can be expressed as

$$i_{\text{t, main}} = i_{\text{hole, main}} + \Delta i_{<100>} \quad (6)$$

while at the tips of side pores the current density is

$$i_{\text{t, side}} = i_{\text{hole, side}} \cos \theta + \Delta i_{<100>} \sin \theta \quad (7)$$

Side pores grow at an angle, $\tan\theta = \Delta i_{<100>} / i_{\text{hole, side}}$, from the growth direction of the main pores. When the side pores become normal to the main pores when $\Delta i_{<100>} \gg i_{\text{hole, side}}$, dendritic PS is formed. Also, when $i_{\text{hole, main}} \gg i_{\text{hole, side}}$ the side pores do not grow very long before growth stops as the tip of the main pore quickly advances such that the material near the bottom of the side pores are quickly depleted of carriers. Little branching occurs under such a condition.

The stability of the profile of the pore bottom against local current perturbations determines the straightness of pores. Assume the amount of material dissolved, Δm , due to a current perturbation on a pore bottom, Δi , is $\Delta m = A\Delta i \cdot t$ where t is time and A is a constant. This amount of dissolution may cause only a small change in the bottom profile of a large pore but can significantly change that of a small pore and may alter the growth direction of the small pore. This is why large pores are generally straighter than small pores because the bottom profile of large pores are more stable against random perturbations in the system.

(v) *Two-Layer PS*

Two-layer PS with a micro PS on top of a macro PS layer is formed on lowly doped p-Si or illuminated n-Si. For lowly doped p-Si two-layer PS can form when the conditions are such that the space charge layer and the resistive layer differ in dimension by several orders of magnitude.

Figure 28 illustrates schematically the two-layer PS formed on illuminated n-Si. The photo generated holes are located near the surface and flow to various directions depending on the direction of the field inside the walls of the micro PS (Note that the walls in these micro PS, in the order of nanometers, are much smaller than the thickness of space charge layer). These photo carriers can result in the dissolution of PS without the assistance of an applied anodic potential and are responsible for the etching of the PS layer. On the other hand, the photo carriers generated at different depths within the space charge layer are collected at the surface of the macro pore, resulting in the formation and growth of the micro PS on the surface of macro pore. The holes that are generated beyond the space charge layer are mostly collected and

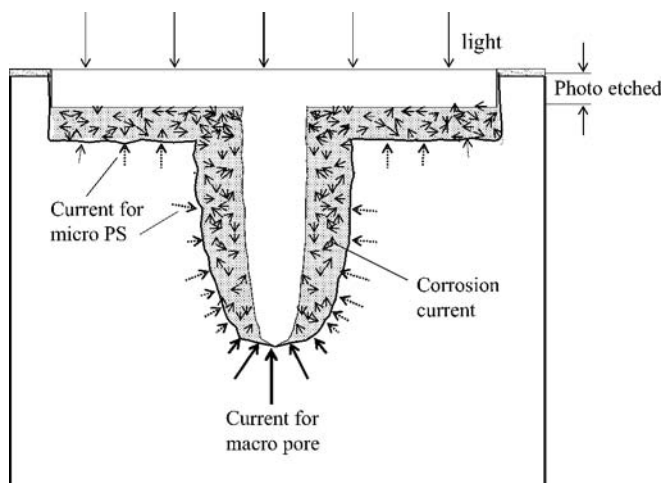


Figure 28. Schematic illustration of formation of a macro pore partially filled by a micro PS on n-Si under illumination.

react at the bottom of the macro pore resulting in the growth of the macro pore. Also, depending on the current density relative to that required for the formation of oxide, the tip area may or may not be covered with an oxide film. When the entire pore bottom is not covered with oxide, the macro pores will be fully filled with micro PS. On the other hand, when the tip area of pores is partially covered with an oxide film, macro pores are only partially filled with micro PS.

The formation of two-layer PS on p-Si involves two different physical layers in which the potential-current relations are sensitive to the radius of curvature. The space charge layer of p-Si under an anodic potential is thin, which is responsible for the formation of the micro PS. The non-linear resistive effect of the highly resistive substrate is responsible for that of macro PS. The effect of high substrate resistivity should also occur for lowly doped n-Si. However, under normal conditions, the thickness of the space charge layer under an anodic potential, at which macro PS is formed, is on the same order of magnitude as the dimension

of the resistive layer. The effect of these two different causes on the pore diameter is thus not normally distinguishable. If the conditions can be controlled such that the pores formed due to the effect of the space charge layer and those formed due to the effect of the resistive layer have a size difference by at least one order of magnitude it could be possible to obtain two-layer PS on n-Si.

For macro pores at a stable growth condition, the distribution of current density on the surface of an individual pore bottom is bell-like as shown in Figure 29a. For micro PS, the pores tend to grow in a zigzag fashion and the distribution of current at the dissolution front of PS is highly modulated across the surface as illustrated in Figure 29b. For two-layer PS, in which macro pores can be filled or partially filled with micro PS, the current profiles are illustrated in Figure 29c and 29d. The bell-shape distribution of the current responsible for growth of macro pores is consisted of fine modulations of the current responsible for growth of micro PS. When the current densities are such that no oxide occurs on any area of the pore bottom the macro pore is fully filled by micro PS. On the other hand, when the current density is such that oxide forms at the tip, the macro pore is only partially filled by micro PS.

(vi) Dissolution of PS During its Formation

The dissolution of PS during PS formation may occur in the dark or under illumination. Both are essentially corrosion processes, by which the silicon in the PS is oxidized and dissolved with simultaneous reduction of the oxidizing species in the solution. The material in the PS, which is distant from the growing front is little affected by the external bias due to the high resistivity of PS and is essentially at the open circuit potential (OCP). Such corrosion process is responsible for the formation of micro PS of certain thickness (stain film) in HF solutions containing oxidants under an unbiased condition.

Because the dissolution of silicon in HF solution requires holes, the corrosion rate of silicon in HF solutions at OCP is very low due to the unavailability of holes. But due to the large surface area of PS, the amount of dissolution still has a significant effect on the density of PS (e.g., PS density decreases with increasing PS thickness).

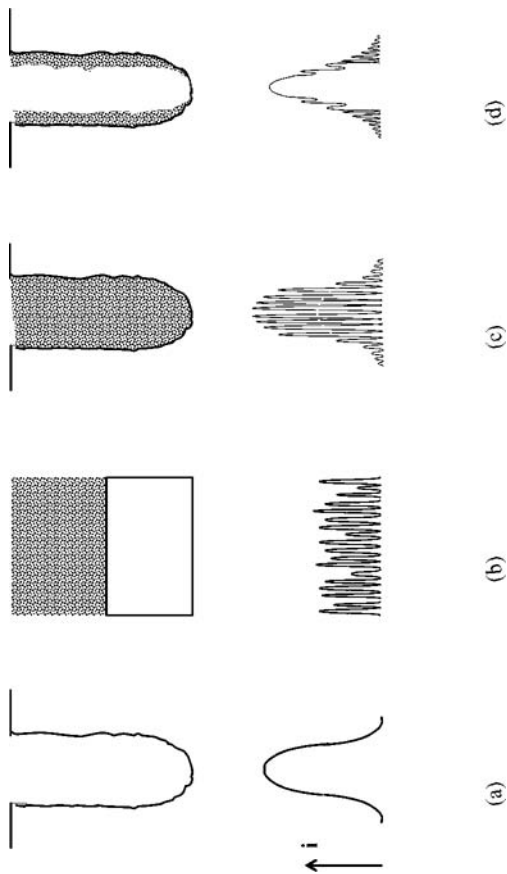


Figure 29. Schematic illustration for different types of PS and the current distributions; (a) void macro pore (b) micro PS (c) macro pore filled with micro PS (d) macro pore partially filled with micro PS.

Illumination generates holes within the material of PS and causes photo corrosion of PS that is much faster than that in the dark. Depending on illumination intensity and time, the pore walls in a PS can be thinned to various extents by the photo induced corrosion. This corrosion process is responsible for the etched crater between the initial surface and the surface of PS as illustrated in Figure 28. It is also responsible for the fractal structure of the micro PS formed under illumination.

V. SUMMARY

This chapter provided a conceptual analysis of the various aspects of morphology and formation mechanisms of porous silicon based on available information on the fundamental reaction processes on the silicon/electrolyte interface. According to the global mechanistic scheme described, the diverse types of PS can be categorized into three groups: 1) space charge layer controlled. This includes all PS except for the macro PS formed on p-Si. The diameter of the pores in these PS types is comparable to the width of space charge layer; 2) substrate resistance controlled. This includes the macro PS formed in lowly doped p-Si and possibly on lowly doped n-Si (a prediction); 3) photo carrier controlled. This includes all micro PS in single and two-layer PS formed under illumination.

Some morphological features of porous silicon in relation to formation condition as defined by the kinetics according to current and HF concentration are illustrated Figure 30. The lines defining the regions are determined by the nature of the reactions and are independent of the doping type and concentration (see Figure 4). One important factor governing the change of one region to the other is the formation and coverage of an anodic oxide film on the surface. The coverage of oxide on the surface increases from zero in PS region A to only at pore tips in PS region B to part of the surface in the transition region to full coverage in the electropolishing region.

Formation of porous silicon is an anodic dissolution process, which consists of carrier transport in the semiconductor, electrochemical reactions at the interface, and mass transport of the reactants and reaction products in the electrolyte. There are a

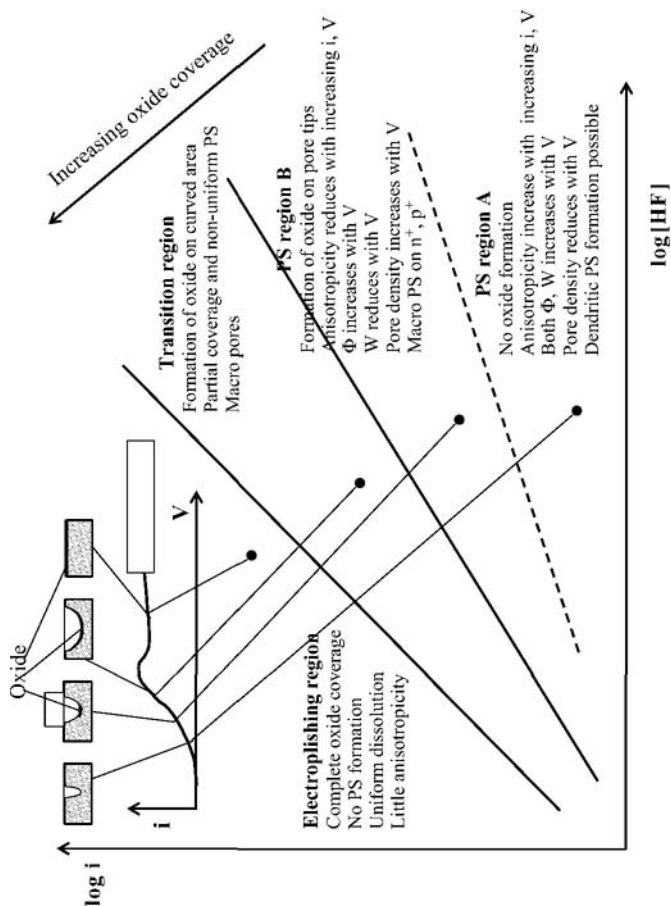


Figure 30. Conditions for the formation of various morphological features of PS.

number of reactions involved at the interface and these reactions consist of several steps and sub-reactions. At any given time, the dissolution kinetics can be controlled by any one or several of these steps. The distribution of reactions along a pore bottom under a steady state condition during pore propagation must be such that pore walls are relatively less active than the pore tip. Then, the dissolution reactions are concentrated at the pore tip to result in the preferential dissolution and the formation of pores. The formation of pores is the consequence of spatially and temporally distributed reactions.

The fundamental reason for the uneven distribution of reactions is that the rate of electrochemical reactions on a semiconductor is sensitive to the radius of curvature of the surface. This sensitivity can either be associated with the thickness of the space charge layer or the resistance of the substrate. Thus, when the rate of the dissolution reactions depends on the thickness of the space charge layer, formation of pores can in principle occur on a semiconductor electrode. The specific porous structures are determined by the spatial and temporal distributions of reactions and their rates which are affected by the geometric elements in the system. Because of the intricate relations among the kinetic factors and geometric elements, the detail features of PS morphology and the mechanisms for their formation are complex and greatly vary with experimental conditions.

REFERENCES

1. X. G. Zhang, *Electrochemistry of Silicon and Its Oxide*, Kluwer Academic, New York, 2001
2. D. R. Turner, *J. Electrochem. Soc.*, **105** (1958) 402.
3. A. Uhlir, Jr., *The Bell System Technical Journal*, **March** (1956) 333.
4. R. Memming and G. Schwandt, *Surf. Sci.* **4** (1966) 109.
5. R. L. Meek, *J. Electrochem. Soc.*, **118** (1971) 437.
6. M. J. J. Theunissen, *J. Electrochem. Soc.*, **119** (1972) 351.
7. Y. Arita and Y. Sunahama, *J. Electrochem. Soc.*, **124** (1977) 285.
8. Y. Watanabe, Y. Arita, T. Yokoyama and Y. Lgarashi, *J. Electrochem. Soc.*, **122** (1975) 1315.
9. G. Bonchil, R. Herino, K. Barla and J. C. Pfister, *J. Electrochem. Soc.*, **130** (1983) 1611.
10. T. Uganami and M. Seki, *J. Electrochem. Soc.*, **125** (1978) 1339.
11. V. Labunov, I. Baranov and V. Bondarenko, *Thin Solid Film*, **64** (1979) 479.

12. M. I. J. Beale, J. D. Benjamin, M. J. Uren, N. G. Chew, and A. G. Cullis, *J. Crystal Growth*, **73** (1985) 622.
13. S. F. Chuang, S. D. Collins, and R. L. Smith, *Appl. Phys. Lett.*, **55**(7), 14 August, (1989) 675.
14. R. L. Smith and S. D. Collins, *J. Appl. Phys.* **71**(8), 15 April, (1992) R1.
15. R. L. Smith, S. F. Chuang, and S. D. Collins, *J. Electronic Materials*, **17** (1988) 228.
16. T. Unagami, *J. Electrochem. Soc.*, **127** (1980) 476.
17. V. P. Parkhutik, L. K. Glinenko, and V.A. Labunov, *Surface Technology*, **20** (1983) 265.
18. X. G. Zhang, S. D. Collins, and R. L. Smith, *J. Electrochem. Soc.*, **136** (1989) 1561.
19. V. Lehmann, *J. of Electroanalytical Chemistry*, **140** (1993) 2836.
20. V. Lehmann and H. Foll, *J. Electrochem. Soc.*, **137** (1990) 653.
21. V. Lehmann, *Thin Solid Films*, **255** (1995) 1.
22. V. Lehmann and U. Gosele, *Advanced Materials*, **4** (1992) 114.
23. V. Lehmann and U. Gosele, *Appl. Phys. Lett.*, **58**(8), 25 February, (1991) 856.
24. X.G. Zhang, *J. Electrochem. Soc.*, **138** (1991) 3750.
25. M. H. Al Rifai, M. Christophersen, S. Ottow, J. Carstensen, and H. Foll, *J. Electrochem. Soc.*, **147** (2000) 627.
26. T. Osaka, K. Ogasawara, and S. Nakahara, *J. Electrochem. Soc.*, **144** (1997) 3226.
27. C. Levy-Clement, A. Lagoubi and M. Tomkiewicz, *J. Electrochem. Soc.*, **141** (1994) 958.
28. C. Levy-Clement, A. Lagoubi, R. Tenne and M. Neumann-Spallart, *Electrochimica Acta*, **37**(5) (1992) 877.
29. A. A. Yaron, S. Bastide, J. L. Maurice and C. L. Clément, *J. Luminescence*, **57** (1993) 67.
30. Y. Arita, *Journal of Crystal Growth*, **45** (1978) 383.
31. C. Levy-Clement, A. Lagoubi, and M. Tomkiewicz, *J. Electrochem. Soc.*, **141** (1994) 958.
32. M. M. Rieger and P. A. Kahl, *J. Electrochem. Soc.*, **142** (1995) 1490.
33. E. K. Propst and P. A. Kohl, *J. Electrochem. Soc.*, **141** (1994) 1006.
34. E. A. Ponomarev and C. Levy-Clement, *Electrochemical and Solid-State Letters*, **1** (1998) 42.
35. R. B. Wehrspohn, J. -N. Chazalviel, and F. Ozanam, *J. Electrochem. Soc.*, **145** (1998) 2958.
36. S. Cattarin, E. Pantano, and F. Decker, *Electrochemistry Communications*, **1** (1999) 483.
37. J. -N. Chazalviel, R. B. Wehrspohn, and F. Ozanam, *Materials Science and Engineering*, **B69-70** (2000) 1.
38. R. B. Wehrspohn, F. Ozanam, and J. -N. Chazalviel, *J. Electrochem. Soc.*, **146** (9) (1999) 3309.
39. V. Lehmann and S. Ronnebeck, *J. Electrochem. Soc.*, **146** (1999) 2968.
40. J. Carstensen, M. Christophersen, and H. Foll, *Materials Science and Engineering*, **B69-70** (2000) 23.
41. H. Foll, J. Carstensen, M. Christophersen, and G. Hasse, *Physica Status Solidi*, **a(182)** (2000) 45

- 42 J. Carstensen, M. Christophersen, and H. Foll, *Physica Status Solidi*, (2000) 63.
- 43 G. Hasse, M. Christophersen, J. Carstensen, and H. Foll, *Physica Status Solidi*, a(182) (2000) 23.
- 44 P. Jaguiro, S. La Monica, S. Lazarouk and A. Ferrari, *Electrochemical Society Proceedings*, **97-7** (1997) 296.
- 45 A. Valance, *Physical Review B*, **55** (1997) 9706.
- 46 S. La Monica, P. Jaguiro, and A. Ferrari, *Electrochemical Society Proceedings*, **97-7** (1997) 140.
- 47 R. S. Muller and T. I. Kamins, *Device Electronics for Integrated Circuits*, John Wiley & Sons, New York, 1977.
- 48 I. Ronga, A. Bsiesy, F. Gaspard, F. Herino, M. Ligeon, and F. Muller, *J. Electrochem. Soc.*, **138** (1991) 1403.
- 49 F. Gaspard, A. Bsiesy, M. Ligeon, F. Muller, and R. Herino, *J. Electrochem. Soc.*, **136** (1989) 3043.
- 50 P. C. Searson and X. G. Zhang, *J. Electrochem. Soc.*, **137** (1990) 2539.
- 51 Y. Kang and J. Jorne, *J. Electrochem. Soc.*, **144**(9) (1997) 3104.
- 52 M. J. Eddowes, *J. Electroanal. Chem.*, **280** (1990) 297.
- 53 V. A. Burrows, Y. J. Chabal, G. S. Higashi, K. Raghavachari and S. B. Christman, *Appl. Phys. Lett.*, **53**(11) (1988) 998.
- 54 C. M. Gronet, N. S. Lewis, G. Cogan, and J. Gibbons, *Proc. Natl. Acad. Sci. USA*, **80** (1983) 1152.
- 55 S. Lust and C. Levy-Clement, *J. Electrochem. Soc.*, **149** (2002) C338.
- 56 E. Peiner, and A. Schlachetzki, *J. Electrochem. Soc.*, **139** (1992) 552.
- 57 J. Rappich and H.J. Lewerenz, *Thin Solid Film*, **276** (1996) 25.
- 58 J.-N. Chazalviel, M. Etman, and F. Ozanam, *J. Electroanal. Chem.*, **297** (1991) 533.
- 59 P.C. Searson, J.M. Macaulay, and Prokes, *J. Electrochem. Soc.*, **139** (1992) 3373.
- 60 R. Herino, G. Romchil, K. Boala, and C. Bertrand, *J. Electrochem. Soc.*, **134** (1987) 1994.
- 61 I. Ronga, A. Bsiesy, F. Gaspard, F. Herino, M. Ligeon, and F. Muller, *J. Electrochem. Soc.*, **138** (1991) 1403.
- 62 V. V. Doan and M. Sailor, *Science*, **256** (1992) 1791.
- 63 M. Christophersen, J. Carstensen, A. Feuerhake, and H. Foll, *Materials Science and Engineering*, **B69-70** (2000) 194.
- 64 L. Koker and K. W. Kolasinski, *Materials Science and Engineering*, **B69-70** (2000) 132.
- 65 X. G. Zhang, unpublished results.
- 66 R. C. Frye, *Mat. Res. Soc. Symp. Proc.*, **33** (1984) 53.
- 67 M. Guendouz, P. Joubert, and M. Sarret, *Materials Science and Engineering*, **B69-70** (2000) 43.
- 68 H. Unno, K. Imai, and S. Muramoto, *J. Electrochem. Soc.*, **134** (1987) 645.
- 69 H. Braumgart, R. C. Frye, F. Philipp, and H. J. Leamy, *Mat. Res. Soc. Symp. Proc.* **33** (1984) 63.
- 70 O. Teschke, *Appl. Phys. Lett.*, **64**(15) (1994) 1986.
- 71 M. I. J. Beale, N. G. Chew, M. J. Uren, A. G. Cullis, and J. D. Benjamin, *Appl. Phys. Lett.*, **46**(1) (1985) 1095.
- 72 H. Sugiyama and O. Nittono, *Journal of Crystal Growth*, **103** (1990) 156.

- 73 K. D. Legg, A. B. Ellis, J. M. Bolts, and M. S. Wrighton, *Proc. Natl. Acad. Sci. USA*, **74**(10) (1977) 4116.
- 74 N. Noguchi, I. Suemune, M. Yamanishi, G. C. Hua, and Nobuo Otsuka, *Jpn. J. Appl. Phys.*, **31** (1992) L490.
- 75 M. Christophersen, J. Carstensen, and H. Foll, *Physica Status Solidi*, (a) **182**, 1 (2000) 45.
- 76 S. -F. Chuang, S. D. Collins, and R. L. Smith, *Appl. Phys. Lett.*, **55**(15) (1989) 1540.
- 77 P. C. Searson, J. M. Macaulay, and F. M. Ross, *J. Appl. Phys.*, **72**(1) (1992) 253.
- 78 T. Osaka, K. Ogasawara, M. Katsunuma, and T. Momma, *J. of Electroanalytical Chemistry*, **396** (1995) 69.
- 79 V. Labunov, V. Bondarenko, L. Glinenko, A. Dorofeev and L. Tabulina, *Thin Solid Films*, **137** (1986) 123.
- 80 V. Lehmann, R. Stengl, and A. Luigart, *Materials Science and Engineering*, **B69** (2000) 11.
- 81 V. Lehmann, A. Luigart and V. Corbel, *Electrochemical Society Proceedings*, **97-7** (1997) 132.
- 82 C. Gui, M. Elwenspoek, J. G. E., Gardeniers, and P. V. Lambeck, *J. Electrochem. Soc.*, **145** (1998) 2204.
- 83 E.A. Ponomarev and C. Levy-Clement, *Electrochemical Society Proceedings*, **97-7** (1997) 319.
- 84 C. Jäger, B. Finkenberger, W. Jäger, M. Christophersen, J. Carstensen, and H. Föll, *Materials Science and Engineering*, **B69-70** (2000) 199.
- 85 V. Lehmann and U. Grüning, *Thin Solid Films*, **297** (1997) 13.
- 86 J. E. A. M. van den Meerakker, R. J. G. Elfrink, F. Roozeboom and J. F. C. M. Verhoeven, *J. Electrochem. Soc.*, **147**(7) (2000) 2757.
- 87 P. Allongue, C. H. de Villeneuve, M. C. Bernard, J. E. Peou, A. Boutry-Forveille, and C. Levy-Clement, *Thin Solid Films*, **297** (1997) 1.
- 88 St. Frohnhoff, M. Marso, M. G. Berger, M. Thonossen, H. Luth, and H. Munder, *J. Electrochem. Soc.*, **142** (1995) 615.
- 89 M. Binder, T. Edelmann, T. H. Metzger, G. Mauckner, G. Goerigk, and J. Peisl, *Thin Solid Film*, **276** (1996) 65.
- 90 S. Billat, M. Thonissen, R. Arens-Fischer, M. G. Berger, M. Kruger, and H. Luth, *Thin Solid Films*, **297** (1997) 22.
- 91 R. Houbertz, U. Memmert, and R. J. Behm, *J. Vac. Sci. Technol. B*, **12**(6) (1994) 3145.
- 92 M. Thönissen, M. G. Berger, R. Arens-Fischer, O. Glüger, and H. Lüth, *Thin Solid Films*, **276** (1996) 21.
- 93 M. Thönisson, M. G. Berger, R. Arens-Fisher, O. Glück, M. Krüger, and H. Lüth, *Thin Solid Film*, **276** (1996) 21.
- 94 S. F. Chuang, S. D. Collins and R. L. Smith, *The Technical Digest of the Solid State Sensor and Actuator Workshop*, Hilton Head Island, SC, June 6-9, IEEE, New York, 1988, p.151.
- 95 S. Ronnebeck, J. Carstensen, S. Ottow, and H. Foll, *Electrochemical and Solid State Letters*, **2** (2000) 126.
- 96 S. Bengtsson and L. Engstrom, *J. Appl. Phys.*, **66**(3) (1989) 1231.
- 97 A. G. Cullis and L. T. Canham, *Nature*, **353** (1991) 353.
- 98 A. Belaidi, M. Safi, F. Ozanam, J. N. Chazalviel, and O. Gorochov, *J. Electrochem. Soc.*, **46** (1999) 2659.

Modern Aspects of Electrochemistry 39

Vayenas, C.G.; White, R.E. (Eds.)

2006, XXI, 279 p., Hardcover

ISBN: 978-0-387-23371-0